Predictions of the glass transition temperature and viscosity of organic aerosols from volatility distributions

Ying Li[1,*], Douglas A. Day[2,3], Harald Stark[2,3,4], Jose L. Jimenez[2,3] and Manabu Shiraiwa[1,*]

[1] Department of Chemistry, University of California, Irvine, CA 92697-2025, USA

[2] Cooperative Institute for Research in Environmental Sciences (CIRES), University of Colorado, Boulder, CO 80309, USA

[3] Department of Chemistry, University of Colorado, Boulder, CO 80309, USA

[4] Aerodyne Research Inc., Billerica, Massachusetts 01821, USA

[*]Correspondence to: Ying Li (yingl47@uci.edu) or Manabu Shiraiwa (m.shiraiwa@uci.edu)

Abstract:

Volatility and viscosity are important properties of organic aerosols (OA), affecting aerosol processes such as formation, evolution and partitioning of OA. Volatility distributions of ambient OA particles have often been measured, while viscosity measurements are scarce. We have previously developed a method to estimate the glass transition temperature (T_g) of an organic compound containing carbon, hydrogen, and oxygen. Based on analysis of over 2400 organic compounds including oxygenated organic compounds as well as nitrogen- and sulfur-containing organic compounds, we extend this method to include nitrogen- and sulfur-containing compounds based on elemental composition. In addition, parameterizations are developed to predict T_g as a function of volatility and the atomic oxygen-to-carbon ratio based on a negative correlation between T_g and volatility. This prediction method of T_g is applied to ambient observations of volatility distributions at eleven field sites. The predicted T_g of OA under dry conditions vary mainly from 290 K to 339 K and the predicted viscosities are consistent with the results of ambient particle phase state measurements in the southeastern US and the Amazonian rain forest. Reducing the uncertainties in measured volatility distributions would improve predictions of viscosity especially at low relative humidity. We also predict the T_g of OA components identified via positive matrix factorization of aerosol mass spectrometer data. The predicted viscosity of oxidized OA is consistent with previously reported viscosity of SOA derived from α-pinene, toluene, isoprene epoxydiol (IEPOX), and diesel fuel. Comparison of the predicted viscosity based on the observed volatility distributions with the viscosity simulated by a chemical transport model implies that missing low volatility compounds in a global model can lead to underestimation of OA viscosity at some sites. The relation between volatility and viscosity can be applied in the molecular corridor or volatility basis set approaches to improve OA simulations in chemical transport models by consideration of effects of particle viscosity in OA formation and evolution.

1. Introduction

Organic aerosols (OA) contribute substantially to the mass loadings of atmospheric fine particulate matter (Hallquist et al., 2009; Jimenez et al., 2009). OA formed from various anthropogenic or biogenic precursors have complex physicochemical properties (Goldstein and Galbally, 2007; Nizkorodov et al., 2011; Ditto et al., 2018), which makes predictions of their role in air quality, climate and public health challenging (Kanakidou et al., 2005; Shrivastava et al., 2017). Volatility and viscosity are important properties of OA, both of which affect important aerosol processes such as gas–particle partitioning, new particle formation and evolution of size distribution, heterogeneous reactions, and cloud condensation and ice nucleation pathways of OA, as summarized in recent review articles (Krieger et al., 2012; Bilde et al., 2015; Pöschl and Shiraiwa, 2015; Knopf et al., 2018; Reid et al., 2018).

Recent measurements have shown that OA can exist in liquid (low dynamic viscosity η; $\eta < 10^2$ Pa s), semi-solid ($10^2 \leq \eta \leq 10^{12}$ Pa s), and amorphous solid ($\eta > 10^{12}$ Pa s) states, depending on temperature (T), relative humidity (RH), and chemical composition (Reid et al., 2018). Even though there are several particle bounce measurements to infer ambient OA phase state, there are limited ambient measurements of particle phase state or viscosity (Virtanen et al., 2010; O'Brien et al., 2014; Bateman et al., 2016; Pajunoja et al., 2016; Bateman et al., 2017; Liu et al., 2017; Ditto et al., 2019; Slade et al., 2019). Viscosity can be directly converted to bulk diffusivity of organic molecules using the Stokes–Einstein equation, which has been shown to work well for organic molecules diffusing through low viscous materials (Price et al., 2016; Chenyakin et al., 2017). This relation is inapplicable for predicting the bulk diffusivity of water and small molecules and it may also underestimate the diffusivity of organic molecules in a highly viscous matrix, which can be corrected using a fractional Stokes-Einstein equation (Price et al., 2016; Evoy et al., 2019).

Viscosity can be related to the glass transition temperature (T_g), at which a phase transition between amorphous solid and semi-solid states occurs (Koop et al.,

74	2011). Ambient temperature varies through 100 K throughout the troposphere, greatly

75	influencing the viscosity of the mixture. When the ambient temperature is below T_g, an

76	amorphous particle behaves as a solid, while a particle would be semi-solid or liquid

77	when the ambient temperature is above T_g. OA particles contain a number of organic

78	compounds and also a variable amount of liquid water depending on RH, which can act

79	as a plasticizer to reduce T_g: these mixture effects can be estimated using the Gordon-

80	Taylor relation (Mikhailov et al., 2009; Koop et al., 2011; Dette et al., 2014). In

81	addition, ambient OA may often be internally mixed with inorganic species such as

82	sulfate and nitrate, which would further lower T_g and viscosity if they are well-mixed

83	in one phase; when the phase separation occurs, the inorganic-rich and organic-rich

84	phases may undergo glass transition at different temperatures (Dette and Koop, 2015).

85	For pure organic compounds with known molecular structure, viscosity can

86	be predicted by group contribution approaches (Cao et al., 1993; Bosse, 2005; Song et

87	al., 2016b; Rovelli et al., 2019; Gervasi et al., 2020); chemical composition of ambient

88	OA is complex and molecular specificity is often unavailable, which makes viscosity

89	predictions of ambient OA challenging. We have recently developed a set of semi-

90	empirical parameterizations using molar mass (M) and atomic O:C ratio (Shiraiwa and

91	Li et al., 2017) or elemental composition (DeRieux and Li et al., 2018) to predict T_g for

92	compounds comprised of carbon, hydrogen, and oxygen (CHO compounds). These

93	parameterizations have been applied to high-resolution mass spectrometry

94	measurements to estimate viscosity of organic aerosols (DeRieux and Li et al., 2018;

95	Schum et al., 2018; Ditto et al., 2019; Song et al., 2019) and coupled into a

96	thermodynamic model (Gervasi et al., 2020). Note that heteroatoms and the effects of

97	molecular structure and functional groups on T_g are not considered in parameterizations

98	of Shiraiwa and Li et al. (2017) and DeRieux and Li et al. (2018).

99	Viscosity of pure compounds has been found to be inversely correlated with

100	vapor pressure (Thomas et al., 1979). The molecular corridor (Shiraiwa et al., 2014; Li

101	et al., 2016) based analysis of hundreds of SOA components has shown that compounds

102 with lower pure compound saturation mass concentration (C^0) have higher T_g (Shiraiwa

103 et al., 2017). Rothfuss & Petters (2017) found that there is a similar trend between the

104 sensitivity of viscosity to functional group addition and the sensitivity of vapor pressure

105 to functional group addition. Measurements of the evaporation kinetics of maleic acid

106 showed that decreasing particle viscosity leads to a suppression in the effective vapor

107 pressure of maleic acid (Marshall et al., 2018). Champion et al. (2019) found secondary

108 organic aerosols (SOA) with higher condensed-phase fractions of extremely low

109 (ELVOC) and low volatile organic compounds (LVOC) showed an increased viscosity.

110 Zhang et al. (2019) measured T_g of isoprene SOA components including isoprene

111 hydroxy hydroperoxide (ISOPOOH), isoprene-derived epoxydiols (IEPOX), 2-

112 methyltetrols, and 2-methyltetrol sulfates (2-MT-OS), observing a tight correlation

113 between T_g and vapor pressure.

114 Based on the above evidence showing a close relation between volatility and

115 viscosity, in this study we develop the parameterizations predicting T_g as a function of

116 C^0 based on data from over 2000 compounds. Functional group contribution approaches

117 are often used to predict C^0 (Capouet and Müller, 2006; Pankow and Asher, 2008;

118 Compernolle et al., 2011; O'Meara et al., 2014), thereby using C^0 to predict T_g would

119 include the molecular structure effect indirectly. The developed parameterizations are

120 applied to field observations of volatility distributions to predict viscosity of ambient

121 OA.

122

123 **2. Methods**

124 **2.1 Dataset of glass transition temperature**

125 The training dataset used to develop the parameterizations of T_g include 2448

126 organic compounds classified into four classes (see the number of CH, CHO, CHON,

127 and CHOS compounds in Table S1). Measured T_g values are available for 42 CH

128 compounds, 259 CHO compounds, 35 CHON compounds and 1 CHOS compound

129 (Koop et al., 2011; Rothfuss and Petters, 2017; Lessmeier et al., 2018; Zhang et al.,

130   2019), among which there are 168 compounds with measured C^0 available (Table S1).

131   When T_g measurements are unavailable, T_g is estimated from the melting temperature

132   (T_m) applying the Boyer-Kauzmann rule of $T_g = g \cdot T_m$ (Kauzmann, 1948; Boyer, 1954)

133   with $g = 0.70085$ (± 0.00375) (Koop et al., 2011), referred to "estimated T_g" in this study

134   (see good agreement of measured and estimated T_g in Fig. S1a). 1187 compounds (391

135   CH, 537 CHO, 241 CHON and 18 CHOS compounds) with both measured T_m and C^0

136   (Table S1, S2) are adopted from the MPBPWIN Program Test Sets

137   (http://esc.syrres.com/interkow/EpiSuiteData.htm) included in the Estimation

138   Programs Interface (EPI) Suite software version 4.1 (US EPA, 2015). Measured T_g, T_m

139   or C^0 for CHOS compounds are sparse and we adopt 850 CHOS compounds included

140   in Li et al. (2016) with their T_m and C^0 estimated by the EPI Suite software (Table S2).

141   There are estimation limitations in the EPI Suite; for example, the disagreement

142   between measured and estimated C^0 is larger for compounds with $C^0 < \sim 10^{-2}$ μg m^{-3}

143   (Fig. S1b), which may affect the T_g predictions for compounds with low volatility.

144   However, given the large amount of data points with measured C^0 included in the

145   training dataset, the estimation bias introduced by the EPI Suite may not substantially

146   impact the accuracy of the parameterization developed in this study.

147   The test dataset used to validate the performance of the parameterizations

148   predicting T_g of SOA components includes 654 CHO compounds and 212 CHON

149   compounds found in SOA oxidation products (Shiraiwa et al., 2014). The values of

150   their C^0 are estimated using the EVAPORATION model (Compernolle et al., 2011).

151   Their T_m values are adopted from the EPI Suite. The T_g predicted by our

152   parameterizations are compared with the T_g estimated from the T_m applying the Boyer-

153   Kauzmann rule in the test dataset.

154

2.2 Parameterizations of T_g as a function of volatility

156   Figure 1a shows a dependence of T_g on C^0 for 2448 organic compounds in

157   the training dataset. The compounds with lower C^0 have higher T_g and the T_g appears

158   to level at around 420 K at $C^0 < \sim 10^{-10}$ µg m^{-3}. The dependence of T_g on the atomic O:C

159   ratio is weaker (Fig. 1a and Fig. S2), in agreement with previous studies (Koop et al.,

160   2011; Shiraiwa et al., 2017). Note that a tight correlation between T_g and the O:C ratio

161   has been observed for oxidation products formed from specific precursors including α-

162   pinene (Dette et al., 2014), n-heptadecane and naphthalene (Saukko et al., 2012). Based

163   on the trend shown in Fig. 1a, we develop a parameterization (Eq. 1) to predict T_g as a

164   function of C^0 and O:C, which are the parameters used in the two-dimensional VBS

165   (2D-VBS) framework (Donahue et al., 2011).

166

167    $T_g = 289.10 - 16.50 \times \log_{10}(C^0) - 0.29 \times [\log_{10}(C^0)]^2 + 3.23 \times \log_{10}(C^0) \text{(O:C)}$ (1)

168

169   The coefficients in Eq. (1) are obtained by fitting the T_g of 2448 compounds in Fig. 1a

170   with multi-linear least squares analysis with 68% prediction and confidence intervals.

171   The predicted T_g by Eq. (1) is plotted in Fig. 1a with the O:C ratios of 0, 0.5, and 1,

172   showing that the predicted dependence of T_g on C^0 follows the trend well in the training

173   dataset. The O:C ratio mainly affects the predicted T_g of volatile or extremely low

174   volatile compounds. Figure 1b shows that the T_g values of those compounds are

175   predicted well by Eq. (1) as indicated by a high correlation coefficient (R) of 0.92. The

176   average absolute value of the relative error (AAVRE, Aiken et al., 2007) is 12%.

177   Equation (1) is further evaluated using the test dataset for SOA components.

178   Figure 1(c) compares T_g predicted by Eq. (1) with estimated T_g from T_m applying the

179   Boyer-Kauzmann rule, showing that Eq. (1) also presents a good performance for

180   predicting T_g of these SOA components with $R = 0.96$ and AAVRE = 6 %. Note that

181   C^0 values of SOA components were estimated using the EVAPORATION model

182   (Compernolle et al., 2011). The T_g values of individual SOA compounds can be

183   predicted within ±20 K as indicated by the prediction band (dotted lines in Fig. 1c);

184   however, this uncertainty may be much smaller for multicomponent SOA mixtures

185   under ideal mixing conditions as indicated in the confidence band (dashed lines, almost

186 overlapping with the 1:1 line) (Shiraiwa and Li et al., 2017; DeRieux and Li et al., 2018;

187 Song et al., 2019).

188   We also develop a parameterization (Eq. 2) predicting T_g as a function of C^0

189 solely, which can be applied to the information available with the one-dimensional VBS

190 framework (1D-VBS; Donahue et al., 2006), and can be used when the O:C ratio is not

191 available in measurements.

192

193     $$T_g = 288.70 - 15.33 \times \log_{10}(C^0) - 0.33 \times [\log_{10}(C^0)]^2 \qquad\qquad (2)$$

194

195 The coefficients in Eq. (2) are obtained following the procedures developing Eq. (1)

196 and the same training dataset is used. Figures S3-S4 show that Eq. (2) gives very similar

197 predictions as Eq. (1) particularly for the compounds with low O:C ratio. As Eq. (1)

198 and (2) are developed based on the compounds with their C^0 higher than $\sim 10^{-20}$ μg m^{-3},

199 Eqs. (1–2) may not be applicable for compounds with $C^0 < \sim 10^{-20}$ μg m^{-3} (Fig. 1a).

200

201 **2.3 Predictions of T_g and viscosity of organic aerosols**

202   For the application of T_g parameterizations in field observations of volatility

203 distributions, T_g for each volatility bin ($T_{g,i}$) is calculated by Eq. (1). The term volatility

204 refers to the effective saturation mass concentration (C^*) and we assume ideal

205 thermodynamic mixing in which case C^* is equal to C^0 (Donahue et al., 2011). Note

206 that there may be additional uncertainty in application of T_g parameterizations (which

207 were developed based on pure compounds) to each volatility bin representing surrogate

208 of complex multicomponent mixtures. The isolines in Fig. 2 show the $T_{g,i}$ predicted by

209 Eq. (1) with the C^* and O:C defined in the 2D-VBS framework. T_g would be below $\sim$

210 250 K for intermediate volatility organic compounds (IVOC; $300 < C^0 < 3 \times 10^6$ μg m^{-}

211 ^{3}), from $\sim$ 260 K to 290 K for semi-volatile organic compounds (SVOC; $0.3 < C^0 < 300$

212 μg m^{-3}), and higher than 300 K for low-volatile organic compounds (LVOC; $3 \times 10^{-4} <$

213 $C^0 < 0.3$ μg m^{-3}) and extremely low-volatile organic compounds (ELVOC; $C^0 < 3 \times 10^{-}$

214   [4] μg m^{-3}). The T_g increases as the O:C ratio increases for SVOC and IVOC, which is

215   consistent with previous studies (Koop et al., 2011; Saukko et al., 2012; Berkemeier et

216   al., 2014). The T_g slightly decreases as the O:C ratio increases for LVOC and ELVOC

217   compounds, which might be due to the uncertainties in Eq. (1) which is derived from a

218   dataset containing fewer LVOC and ELVOC compounds as shown in Fig. 1a, which

219   exhibits lower T_g with higher O:C.

220   The glass transition temperatures of organic aerosols under dry conditions

221   ($T_{g,org}$) are calculated by the Gordon-Taylor equation (Gordon and Taylor, 1952)

222   assuming the Gordon-Taylor constant (k_{GT}) of 1 (Dette et al., 2014):

223

224      $$T_{g,org} = \sum_i w_i\, T_{g,i} \tag{3}$$

225

226   where w_i is the mass fraction in the particle phase for each volatility bin. The Gordon-

227   Taylor approach has been validated for a wide range of mixtures including SOA

228   compounds (Dette et al., 2014; Lessmeier et al., 2018). The Gordon-Taylor approach

229   may fail in the case of adduct or complex formation (Koop et al., 2011), which is highly

230   unlikely in multicomponent mixtures with myriads of SOA compounds with very small

231   individual mole fractions and thus particular interactions between individual

232   compounds are more likely to average out (Shiraiwa et al., 2017); this aspect would

233   need to be investigated in future studies.

234   The phase state of aerosol particles strongly depends on their water content

235   (Mikhailov et al., 2009; Koop et al., 2011). Under humid conditions, the water content

236   in OA can be estimated using the effective hygroscopicity parameter (κ) (Petters and

237   Kreidenweis, 2007). The T_g of organic-water mixtures ($T_g(w_{org})$) at given RH can be

238   estimated using the Gordon-Taylor equation (Gordon and Taylor, 1952):

239

240      $$T_g(w_{org}) = \frac{(1-w_{org})T_{g,w} + \frac{1}{k_{GT}}w_{org}T_{g,org}}{(1-w_{org}) + \frac{1}{k_{GT}}w_{org}} \tag{4}$$

241

where w_{org} is the mass fraction of organics in particles; $T_{g,w}$ is the glass transition

temperature of pure water (136 K, Kohl et al., 2005), and k_{GT} is the Gordon-Taylor

constant for organic-water mixtures which is suggested to be 2.5 (Zobrist et al., 2008;

Koop et al., 2011). Viscosity can then be calculated applying the Vogel-Tammann-

Fulcher (VTF) equation (Angell, 1991): $\eta = \eta_\infty e^{\frac{T_0 D}{T-T_0}}$, where η_∞ is the viscosity at

infinite temperature (10^{-5} Pa s, Angell, 1991), D is the fragility parameter which is

assumed to be 10 (DeRieux and Li et al., 2018), and T_0 is the Vogel temperature

calculated as $T_0 = \frac{39.17\, T_g}{D+39.17}$.

3. Application in field observations

3.1 Southern Oxidant and Aerosol Study (SOAS)

In this section we predict glass transition temperatures and phase state of

ambient OA during the SOAS campaign which took place in the southeastern United

States (Centreville, Alabama) in summer 2013 (Carlton et al., 2018). The T_g of organic

aerosols under dry conditions ($T_{g,org}$) is calculated using Eqs. (1) and (3) with measured

volatility distributions. Figure 2 shows the calculated $T_{g,org}$ placed in the 2D-VBS

framework against the average $\log_{10}(C^*)$ calculated by $\sum_i w_i \log_{10}(C_i^*)$ (Kostenidou

et al., 2018) and the measured O:C ratio is from Xu et al. (2015).

Figure 2 shows that $T_{g,org}$ of total OA (TOA) range from 232 K to 334 K,

depending on volatility distributions measured by different methods, while the most

credible predicted $T_{g,org}$ values span in the range of $313-330$ K. The reasons are stated

below by comparing the different methods deriving the C^* distributions. Stark et al.

(2017) used three methods ("Thermograms", "Partitioning" and "Formulas") to derive

volatility distributions applying the measurements of organic acids (which were shown

to account for about half of the total OA; Yatavelli et al., 2015) from a high-resolution

chemical ionization time-of-flight mass spectrometer equipped with a filter inlet for

gases and aerosols (Lopez-Hilfiker et al., 2014; Thomson et al., 2017). In the

269   "Thermogram" method, C^* at 298 K is estimated from the desorption temperature after

270   calibration with known species (Faulhaber et al., 2009). This method results in 93% of

271   OA mass distributed in the LVOC and ELVOC (Stark et al., 2017), and a high $T_{g,org}$ of

272   330 K is predicted (Fig. 2). While this method may be influenced by thermal

273   decomposition, the peak temperatures of decomposing species can be expected to relate

274   closer to actual volatilities than any of the other two analysis methods (Stark et al.,

275   2017). The result from the thermogram method is consistent with those measured by an

276   aerosol mass spectrometer (AMS) with a thermo denuder, which also applied the

277   thermogram method to estimate the C^* distributions (Hu et al., 2016). Saha et al. (2017)

278   applied an evaporation kinetic model (Lee et al., 2011) based on the VBS approach to

279   extract the C^* distributions, and the effects of enthalpy of vaporization and

280   accommodation coefficient (α) are considered, resulting in the estimated $T_{g,org}$ of 313

281   K. This study retrieved α of ~0.5, which is consistent with recent experiments

282   (Krechmer et al., 2017; Liu et al., 2019).

283   The lower $T_{g,org}$ values (< 280 K) calculated from the C^* distributions

284   estimated from the "Formulas" and "Partitioning" methods (Stark et al., 2017) are less

285   atmospherically relevant. The "Formulas" method used the SIMPOL group

286   contribution method (Pankow and Asher, 2008) to calculate vapor pressures from the

287   composition of the identified ions. While the specific functional group distributions

288   needed for SIMPOL are unknown from mass spectrometer measurements, some

289   assumptions can be made, leading to limits in the volatility distributions, all of which

290   showing the same behavior of high volatilities (Stark et al., 2017). This is because many

291   of the detected species can be thermal decomposition products rather than actual SOA

292   molecules (Stark et al., 2015; Stark et al., 2017), which can lead to overestimations of

293   volatilities, resulting in the unlikely low $T_{g,org}$ of 232 K. The "Partitioning" method used

294   the measured particle-phase mass fractions of each species to estimate C^* based on the

295   partitioning theory (Pankow, 1994). The estimated C^* is distributed mainly in the

296   SVOC range (Stark et al., 2017), leading to a $T_{g,org}$ of 279 K (Fig. 2). This value is very

close to the $T_{g,org}$ (281 K) simulated by a global chemical transport model EMAC-ORACLE in which a narrow distribution of C^* (1, 10, 10^2, and 10^3 µg m^{-3}) was applied (Shiraiwa et al., 2017). However, Stark et al. (2017) note that the partitioning-based volatility distribution is likely too high due to an artifact of signal-to-noise limitations, confining the C^* characterizable by the partitioning method to a relatively narrow range centered around the ambient OA concentration (by definition, the semi-volatile range). These analyses indicate that the volatility distributions derived from different methods, even when based on the same measurements, significantly affect the predicted $T_{g,org}$, and the most atmospherically relevant volatility distributions should be carefully chosen to reasonably predict the glass transition temperature of ambient OA. In summary, the $T_{g,org}$ values during the SOAS campaign should be in the range of 313 – 330 K.

Figure 2 also includes $T_{g,org}$ of isoprene-epoxydiols-derived SOA (IEPOX-SOA) identified via positive matrix factorization (PMF) of AMS mass spectra (Lanz et al., 2007). IEPOX-SOA is predicted to have a $T_{g,org}$ of 345 K with very low volatility with the average C^* lower than 10^{-4} µg m^{-3} (Hu et al., 2016; Lopez-Hilfiker et al., 2016; D'Ambro et al., 2019), which may be due to substantial formation of organosulfates and other oligomers (Lin et al., 2012; Hu et al., 2015; Riva et al., 2019). The predicted $T_{g,org}$ of IEPOX-SOA is higher than previously reported $T_{g,org}$ of 263 - 293 K for monoterpene-derived (α-pinene, Δ^3-carene, myrcene, limonene and ocimene) SOA (Petters et al., 2019).

We further calculate the viscosity of OA based on the $T_{g,org}$ of TOA predicted above in order to compare with the ambient phase state measurements during the SOAS campaign. Figure 3(a) shows the predicted viscosity of total OA at different RH. T is adopted as 298 K, the average value during the SOAS campaign (Hu et al., 2016). The effective hygroscopicity parameter (κ) is set to 0.14 for TOA based on measurements (Cerully et al., 2015). The characteristic timescale of mass transport and mixing by molecular diffusion (τ_{mix}) is also calculated: $\tau_{mix} = d_p^2 / (4\pi^2 D_b)$ (Seinfeld and Pandis,

325   2006), where d_p is the particle diameter and the bulk diffusion coefficient D_b is

326   calculated from the predicted viscosity by the fractional Stokes–Einstein relation (Evoy

327   et al., 2019). We assume the radius of the diffusing molecule of 10^{-10} m and the particle

328   diameter of 200 nm (Shiraiwa et al., 2011). Note that these estimated timescales

329   represent rough estimations, as molecular interactions in complex mixtures are not

330   considered.

331   The viscosity of TOA at RH of 83% (average RH during SOAS) is predicted

332   to be less than 10^2 Pa s with τ_{mix} less than 1 s, which is consistent with the particle

333   bounce measurements suggesting that organic-dominated particles were mostly liquid

334   during the SOAS campaign (Pajunoja et al., 2016). When RH was below ~50% in the

335   sampling inlet, the particles were found to adopt a semi-solid state (Pajunoja et al.,

336   2016), which agrees with the predicted viscosity of $10^7 - 10^{11}$ Pa s and τ_{mix} can be higher

337   than 1 hour at 50% RH (Fig. 3a). The variations in $T_{g,org}$ (313 – 330 K) due to the

338   different measured C^* distributions (Fig. 2) have a more significant impact on the

339   predicted viscosity at low and medium RH (Fig. 3a). When RH is higher than ~70 %,

340   the predicted viscosities calculated from different $T_{g,org}$ values are very close; at high

341   RH the condensed phase water has a larger influence on the phase state than the

342   volatility does, depending on the hygroscopicity of organic aerosols.

343   Figure 3 (b) shows diurnal variations of predicted viscosity of total OA using

344   measured T and RH during the SOAS campaign (Hu et al., 2016). During 10:00 – 20:00

345   when RH < 70 % and T > 298 K, three simulations using different $T_{g,org}$ values predict

346   that total OA occur as semi-solid with the predicted viscosity of $10^2 - 10^7$ Pa s and the

347   mixing times less than 1 hour. Particles are predicted to have low viscosity of < 1 Pa s

348   adopting a liquid phase during nighttime. The lowest viscosity occurs around 5:00 –

349   6:00 with RH > 95 %. Here we did not consider the effects of the diurnal variations of

350   volatility distributions, as they did not vary dramatically over the campaign period

351   (Saha et al., 2017). Besides T and RH, diurnal variation of ambient aerosol phase state

352   also depends on particle chemical composition and mixing states. Organic particles in

353 Amazon were found to be more viscous at night than the daytime due to the influence

354 of biomass burning that may form non-liquid particles (Bateman et al., 2017). Particles

355 in a mixed forest in northern Michigan were also found more viscous at night despite

356 higher RH than the daytime, due to the formation of high molar mass organic

357 compounds and smaller inorganic sulfate mass fractions (Slade et al., 2019). Phase state

358 measurements during daytime and nighttime at Atlanta suggested that the ambient

359 particle phase state was influenced by OA composition, the presence of inorganic ions,

360 aerosol liquid water and particle mixing state (Ditto et al., 2019).

361

362 **3.2 $T_{g,org}$ at 11 global sites**

363 Figure 4 summarizes $T_{g,org}$ at 11 sites where the measured volatility

364 distributions with volatility bins of four or more are available (Table S3). We did not

365 include the data with narrower volatility ranges which may not correctly characterize

366 the properties of ambient SOA (Bilde et al., 2015), and thus may not be appropriate for

367 estimating volatility distributions and it would result in unrealistically low T_g without

368 considering realistically low C^* bins. Note that a narrow VBS may still be useful for

369 efficiency in 3-dimentional chemical transport models for SOA evaporation and

370 condensation under a narrow range of ambient temperature variations (Kostenidou et

371 al., 2018).

372 Figure 4(a) shows the 2D-VBS framework of O:C vs. $\log_{10}C^*$ with the marker

373 fill color representing $T_{g,org}$, whereas the panel (b) shows $T_{g,org}$ vs. $\log_{10}C^*$ with the

374 marker fill color representing O:C. The marker edge color represents OA components

375 identified via positive matrix factorization of AMS mass spectra (Lanz et al., 2007),

376 including biomass burning OA (BBOA), hydrocarbon-like OA (HOA), cooking OA

377 (COA) and oxygenated OA (OOA) which is sometimes further separated into more

378 oxygenated (MO-OOA) and less oxygenated OA (LO-OOA) factors. Note that these

379 different OA factors may often be internally mixed in ambient atmosphere and

380 predicted $T_{g,org}$ and particle viscosity would be irrelevant in such a case. Nevertheless,

381 these predictions can be useful when particles are externally mixed or ambient OA are

382 dominated by a certain OA factor.

383      $T_{g,org}$ of total OA (TOA) varies from 290 K to 339 K. The lower $T_{g,org}$ occurs

384 at Beijing, China in June 2018 (Xu et al., 2019). OA in Beijing was found to be overall

385 more volatile with the particle-phase semi-volatile fraction of 63%. This may be due to

386 the higher total OA mass concentrations in Beijing (Xu et al., 2019), which facilitates

387 greater partitioning of SVOC compounds into the particle phase, leading to a lower

388 $T_{g,org}$. The predicted $T_{g,org}$ of total OA at numerous other sites range between 300 K and

389 320 K, including Paris (Paciga et al., 2016), Mexico city (Cappa and Jimenez, 2010),

390 Centreville (Hu et al., 2016; Saha et al., 2017; Stark et al., 2017), Raleigh (Saha et al.,

391 2017), and Durham (Saha et al., 2018) in southeastern US. The $T_{g,org}$ value (316 K) at

392 220 m downwind from a highway in Durham is higher than the $T_{g,org}$ (309 K) at 10 m

393 downwind from a highway due to the dilution and mixing of traffic-sourced particles

394 with background air and evaporation of semi-volatile species during downwind

395 transport (Saha et al., 2018). The $T_{g,org}$ values are predicted to be high with >320 K at

396 the sites in Athens (Louvaris et al., 2017), Pasadena (Ortega et al., 2016), Colorado

397 Rocky Mountain (Stark et al., 2017) and Amazon (Hu et al., 2016). The $T_{g,org}$ values

398 for MO-OOA in Mexico city and Paris are predicted to be very high at ~350 K,

399 reflecting their very low volatility.

400   Figure 5 shows the OA viscosity variation of OA components against RH.

401 The hygroscopic growth is considered based on hygroscopicity (κ), which is estimated

402 as a function of the O:C ratio (Lambe et al., 2011) when κ was not measured (Table

403 S3). The κ values of OA factors with low O:C ratio, i.e., HOA, COA and BBOA, are

404 estimated to be low (< 0.08); they are predicted to undergo glass transition at RH

405 between 25 % and 68 % and adopt a liquid phase only when RH is very high (~80%).

406 The predicted behavior of BBOA is in line with bounce measurements observing that

407 particles are semisolid in a biomass burning plume (Bateman et al., 2017). OA factors

408   with higher O:C ratios including LO-OOA, MO-OOA, and IEPOX SOA tend to

409   become liquid (viscosity $< 10^2$ Pa s) at intermediate RH (Fig. 5b).

410   There have been growing measurements of RH-dependent viscosity of

411   laboratory-generated SOA formed from different precursors, e.g., isoprene (Song et al.,

412   2015), α-pinene (Abramson et al., 2013; Renbaum-Wolff et al., 2013; Kidd et al., 2014;

413   Pajunoja et al., 2014; Bateman et al., 2015; Zhang et al., 2015; Grayson et al., 2016;

414   Petters et al., 2019), toluene (Song et al., 2016a) and diesel fuel (Song et al., 2019). As

415   the OOA factors characterized from ambient AMS observations may represent ambient

416   SOA (Jimenez et al., 2009), the predicted viscosities of OOA are compared with

417   laboratory measurements of SOA viscosities in Fig. 5b. It shows that the majority of

418   experimental values is well bounded by the predicted viscosities of OOA, represented

419   by the pink shaded area. One exception is the measured viscosity of isoprene SOA is

420   lower than the predicted viscosity of IEPOX SOA at low RH (<30 %). One possible

421   reason is that the isoprene SOA in experiments was formed with high oxidant

422   concentrations with a short reaction time in an oxidation flow reactor in the absence of

423   inorganic seed particles (Song et al., 2015). In ambient environments heterogeneous

424   reactions with acidic sulfate particles forming oligomers are suggested to be an

425   important pathway (Surratt et al., 2010; Lin et al., 2013; Hu et al., 2015; Hu et al., 2016).

426   These particle-phase organosulfates may contribute to a higher viscosity, as indicated

427   by the predicted viscosity of IEPOX-derived organosulfate mixtures with their $T_{g,org}$

428   estimated to be 313 K (Riva et al., 2019). Another reason could be the mass

429   concentrations of isoprene SOA are much higher (100 ~ 1000 μg m^{-3}, Song et al., 2015)

430   compared to ambient OA concentrations (5 μg m^{-3} during SOAS, Stark et al., 2017).

431   Higher mass concentrations can lead to lower viscosity, as more semi-volatile

432   compounds can partition into the particle phase (Grayson et al., 2016; Jain et al., 2018;

433   Champion et al., 2019).

434

435   **4. Comparison with global simulations**

436   Shiraiwa et al. (2017) simulated the global distribution of annual averages of

437   SOA phase state using the chemical transport model EMAC (Jöckel et al., 2006)

438   coupled with the organic aerosol module ORACLE (Tsimpidi et al., 2014). ORACLE

439   uses the 1D-VBS framework with four C^* bins (1, 10, 10^2, and 10^3 µg m^{-3}). To estimate

440   T_g the values of molar mass and O:C ratio were assigned for each volatility bin based

441   on molecular corridors (Shiraiwa et al., 2014). Note that the molar mass assigned for

442   the volatility bin of 1 µg m^{-3} was assumed to have relatively high molar mass to partially

443   compensate for the fact that ORACLE does not consider lower volatility bins with

444   higher molar mass. As shown in Fig. 6, global distributions of T_g /T presented in

445   Shiraiwa et al. (2017) is converted to viscosity using the VTF equation. Figure 6 also

446   includes the viscosity of total OA at the 11 sites by applying measured volatility

447   distributions and the global model simulated 5 years' average T and RH with κ assumed

448   to be 0.1 (Pringle et al., 2010). Figure 6b shows that the predicted viscosities at the 11

449   sites generally agree with the global simulations: the amorphous solid or semi-solid

450   phase occurs over relatively dry areas, including the sites in western US, Mexico City,

451   Beijing and coastal sites in Greece; the lower viscosity occurs in southeastern US and

452   Paris.

453   The global simulations show that the particles are liquid in the Amazon,

454   while they occur as semi-solid in our predictions based on measured volatility

455   distributions (Fig. 6a). The reason of this disagreement may be mainly due to the

456   substantial fraction of low volatility compounds observed in ambient measurements

457   largely missing from global simulations. Hu et al. (2016) observed that 90 % of OA

458   have volatilities lower than 1 µg m^{-3}, which is the lowest C^* bin in the global simulations.

459   The ambient phase state measurements show that for background conditions of the

460   Amazonian tropical forest, particles are mostly liquid, while with the anthropogenic

461   influence including both urban pollution and biomass burning, they occur as semi-solid

462   or glassy (Bateman et al., 2016; Bateman et al., 2017). The volatility distributions were

463   measured in the dry season heavily influenced by biomass burning (Hu et al., 2016),

which can lead to the higher predicted viscosity. Similar cases are observed in Athens

and the two sites in the western US, that our predictions based on volatility distributions

indicate the glassy phase state while the global model predicts the occurrence of a semi-

solid phase.

5. Conclusions and implications

We have developed parameterizations to estimate the glass transition

temperature of organic compounds using saturation mass concentration (C^0) and atomic

O:C ratio. They can be applied to ambient observations of volatility distributions to

estimate viscosity of ambient organic aerosols. The T_g and viscosity prediction method

can be applied in the volatility basis set or the molecular corridor-based approach to

improve OA simulations in chemical transport models by consideration of effects of

particle viscosity on OA formation and evolution (Shiraiwa et al., 2017; Pye et al., 2017;

Schmedding et al., 2019). Most of the current chemical transport models treat particles

as homogeneously well-mixed liquid without considering particle-phase diffusion

limitations, which can lead to bias in simulations of SOA mass concentrations and

evolution of size distributions (Shiraiwa and Seinfeld, 2012; Zaveri et al., 2018). The

SOA simulations applying the VBS framework have not yet included the effects of

viscosity on SOA formation and evolution. When the gas-particle partitioning is limited

by bulk diffusion, kinetic treatments of SOA partitioning may need to be applied

(Perraud et al., 2012; Liu et al., 2016; Yli-Juuti et al., 2017; Li and Shiraiwa, 2019).

Some chamber experiments probing the mixing timescales of SOA particles formed

from isoprene, α-pinene, and limonene did not observe significant kinetic limitations at

moderate and high RH under room temperature (Loza et al., 2013; Ye et al., 2016),

while kinetic limitations of bulk diffusion of organic molecules in β-caryophyllene

SOA have been observed at 75 % RH (Ye et al., 2018), warranting further investigations

on the degree of kinetic limitations in ambient tropospheric conditions. In addition, the

interplay of diffusion limitations and phase separation impacts heterogeneous and

492 multiphase chemistry (Vander Wall et al., 2018; DeRieux et al., 2019; Zhou et al., 2019)

493 and gas-particle partitioning (Zuend and Seinfeld, 2012; Shiraiwa et al., 2013;

494 Freedman, 2017; Pye et al., 2017; Gorkowski et al., 2019a). The particle morphology

495 and the degree of non-ideal mixing and liquid-liquid phase separation can evolve upon

496 atmospheric aging (Gorkowski et al., 2019b). These aspects may also need to be

497 considered for better representation of organic aerosols in future studies.

498

499 **Appendix A: Parameterizations of T_g based on elemental compositions**

500 We recently developed a parameterization (Eq. A1) predicting T_g as a

501 function of the number of carbon (n_C), hydrogen (n_H), and oxygen (n_O) atoms (DeRieux

502 and Li et al., 2018), similar to the formulation used to predict C^0 (Donahue et al., 2011;

503 Li et al., 2016):

504

505 $$T_g = (n_C^0 + \ln(n_C)) \, b_C + \ln(n_H) \, b_H + \ln(n_C) \ln(n_H) \, b_{CH} + \ln(n_O) \, b_O + \ln(n_C) \ln(n_O) \, b_{CO} \quad \text{(A1)}$$

506

507 Values of the coefficients [n_C^0, b_C, b_H, b_{CH}, b_O, and b_{CO}] are [1.96, 61.99, -113.33, 28.74,

508 0, 0] for CH compounds and [12.13, 10.95, -41.82, 21.61, 118.96, -24.38] for CHO

509 compounds. We broaden the parameterizations for CH and CHO compounds (Eq. A1)

510 to the following equations applicable to CHON (Eq. A2) and CHOS compounds (Eq.

511 A3):

512

513 $$T_g = (n_C^0 + \ln(n_C)) \, b_C + \ln(n_O) \, b_O + \ln(n_N) \, b_N + \ln(n_C) \ln(n_O) \, b_{CO} + \ln(n_C) \ln(n_N) \, b_{CN} +$$

514 $$\ln(n_O) \ln(n_N) \, b_{ON} \quad \text{(A2)}$$

515 $$T_g = (n_C^0 + \ln(n_C)) \, b_C + \ln(n_O) \, b_O + \ln(n_S) \, b_S + \ln(n_C) \ln(n_O) \, b_{CO} + \ln(n_C) \ln(n_S) \, b_{CS} + \ln(n_O)$$

516 $$\ln(n_S) \, b_{OS} \quad \text{(A3)}$$

517

518 Values of the coefficients [n_C^0, b_C, b_O, b_N, b_{CO}, b_{CN} and b_{ON}] in Eq. (A2) are [5.34, 31.53,

519 -7.06, 134.96, 6.54, -34.36, -15.35] and [n_C^0, b_C, b_O, b_S, b_{CO}, b_{CS} and b_{OS}] in Eq. (A3)

are [1.12, 68.41, 64.95, 35.77, -12.32, -9.85, 13.80], respectively. These values are obtained by fitting the T_g of CHON and CHOS compounds included in the training dataset (Fig. 1a, Table S1) with multi-linear least squares analysis. Figure A1 (a) shows a fair agreement between the predicted T_g using Eq. (A2) and the measured or otherwise estimated T_g with R of 0.55 and relatively large AAVRE of 16 % for CHON compounds in the training dataset. Figure A1 (b) shows a better prediction performance with R of 0.83 and AAVRE of 9 % for 212 CHON compounds included in the test dataset for SOA components with their T_g estimated by the Boyer-Kauzmann rule using the EPI-estimated T_m. Figure A1 (c) shows that Eq. (A3) performs well for the CHOS compounds included in the training dataset with their T_g estimated by the Boyer-Kauzmann rule using the EPI-estimated T_m ($R = 0.87$, AAVRE = 8 %).

Figure S5 shows the comparison of T_g predicted by the elemental composition (Eqs. A1– A3) with the T_g predicted as a function of C^0 and the O:C ratio (Eq. 1). The agreement between the two sets of parameterizations for nitrogen- and sulfur-containing compounds is not as good as that for CHO compounds, indicating that there are limitations of predicting T_g by the elemental composition for nitrogen- and sulfur-containing compounds with complex elemental compositions and molecular structures. As volatility depends significantly on functional groups contained in a molecule (Pankow and Asher, 2008; Compernolle et al., 2011), predicting T_g by volatility (Eq. 1) indirectly incorporates the molecular structure effects. As there are limited CHON and CHOS compounds with measured T_g available, future experiments measuring more T_g data for nitrogen- and sulfur-containing organics would help improve the T_g parameterizations by elemental composition.

Appendix B: Comparison of T_g predictions with Zhang et al. (2019)

Recently Zhang et al. (2019) developed a semi-empirical parameterization (Eq. B1) using vapor pressure (p_0 in atm) to predict T_g based on measured T_g of 11 SOA compounds:

548

549 $$T_g = 480.1 - \frac{54395}{(log_{10}(p_0)-1.7929)^2+116.49}$$

550 (B1)

551

552 p_0 can be converted to C^0 via $C^0 = (10^6 M p_0)/(RT)$, where R is the ideal gas constant (R

553 $= 8.2 \times10^{-5}$ m^3 atm mol^{-1} K^{-1}), M is the molar mass (g mol^{-1}), and T is the temperature

554 (K). Figure B1 compares the measured T_g included in the training dataset shown in Fig.

555 1a to T_g predicted by (a) C^0 and the atomic O:C (Eq. 1), (b) elemental composition (Eqs.

556 A1-A3), and (c) Eq. (B1) by Zhang et al. (2019). While all three methods perform

557 reasonably well, the predictions using elemental composition (Eqs. A1-A3) show better

558 performance (Fig. B1b) with R of 0.93 and AAVRE of 11 %, respectively.

559   The prediction performance is influenced by the training dataset used

560 developing parameterizations of T_g. The compounds shown in Fig. B1 contain mostly

561 carboxylic acid and hydroxyl functional groups (Koop et al., 2011; Rothfuss and

562 Petters, 2017) and are included in the training dataset used developing Eq. (1) and (Eqs.

563 A1-A3). The training dataset used in Zhang et al. (2019) included 11 organic

564 compounds, and their parameterization predicted T_g of isoprene SOA very well (Zhang

565 et al., 2019), while underpredicted some low-T_g compounds (Fig. B1c). For compounds

566 with their measured T_g higher than 200 K, predictions by Zhang et al. (2019) show good

567 performance and are consistent with the predictions given by Eq. (1) as a function of

568 C^0 and the O:C ratio. Predicted T_g of 2-MT-OS using the three methods are 297 K (Eq.

569 1, as a function of C^0 and the O:C ratio), 275 K (Eq. A3, as a function of the elemental

570 composition) and 280 K (Eq. B1, Zhang et al., 2019), comparable with the measured

571 T_g of 276 $\pm$ 15 K (Zhang et al., 2019).

572   Note that predictions using elemental composition (Eq. A1) overestimate the T_g

573 of phthalate compounds (the star markers in Fig. B1). For instance, the observed T_g of

574 dioctyl phthalate is 194 K (Zhang et al., 2018), while the prediction is higher than 300

575 K (Fig. B1b). The reason is that ester is not an effective functional group to increase

576 viscosity compared to carboxylic acid and hydroxyl (Rothfuss and Petters, 2017).

577 Parameterizations using volatility (Eqs. 1 and B1) improve the predicted T_g of phthalate

578 compounds (Fig. B1a, c). Figure B2 shows compared to the predictions using Eq. (B1)

579 provided in Zhang et al. (2019), predictions by C^0 and the atomic O:C (Eq. 1) and

580 elemental composition (Eq. A1) agree better with the T_g estimated from the Boyer-

581 Kauzmann rule. Future experiments measuring more T_g of SOA components would

582 help verify the T_g predictions by different parameterizations.

583

584 **Author contribution.** YL, JLJ and MS designed the research. YL developed the

585 parameterizations. DAD, HS and JLJ provided measured volatility distributions for

586 the SOAS campaign. YL and MS wrote the manuscript. All authors discussed the

587 results and contributed to manuscript editing.

588

589 **Data availability.** The data used in this study is available in the supplement.

590

598

599 **References:**

600 Abramson, E., Imre, D., Beranek, J., Wilson, J. M. and Zelenyuk, A.: Experimental
601   determination of chemical diffusion within secondary organic aerosol particles,
602   Phys. Chem. Chem. Phys., 15, 2983-2991, https://doi.org/10.1039/c2cp44013j,
603   2013.

Aiken, A. C., DeCarlo, P. F. and Jimenez, J. L.: Elemental analysis of organic species with electron ionization high-resolution mass spectrometry, Anal. Chem., 79, 8350-8358, https://doi.org/10.1021/ac071150w, 2007.

Angell, C.: Relaxation in liquids, polymers and plastic crystals—strong/fragile patterns and problems, J. Non-Cryst. Solids, 131-133, 13-31, https://doi.org/10.1016/0022-3093(91)90266-9, 1991.

Bateman, A. P., Bertram, A. K. and Martin, S. T.: Hygroscopic influence on the semisolid-to-liquid transition of secondary organic materials, J. Phys. Chem. A, 119, 4386-4395, https://doi.org/10.1021/jp508521c, 2015.

Bateman, A. P., Gong, Z., Liu, P., Sato, B., Cirino, G., Zhang, Y., Artaxo, P., Bertram, A. K., Manzi, A. O., Rizzo, L. V., Souza, R. A. F., Zaveri, R. A. and Martin, S. T.: Sub-micrometre particulate matter is primarily in liquid form over Amazon rainforest, Nat. Geosci., 9, 34-37, https://doi.org/10.1038/ngeo2599, 2016.

Bateman, A. P., Gong, Z., Harder, T. H., de Sá, S. S., Wang, B., Castillo, P., China, S., Liu, Y., O'Brien, R. E., Palm, B. B., Shiu, H. W., Cirino, G. G., Thalman, R., Adachi, K., Alexander, M. L., Artaxo, P., Bertram, A. K., Buseck, P. R., Gilles, M. K., Jimenez, J. L., Laskin, A., Manzi, A. O., Sedlacek, A., Souza, R. A. F., Wang, J., Zaveri, R. and Martin, S. T.: Anthropogenic influences on the physical state of submicron particulate matter over a tropical forest, Atmos. Chem. Phys., 17, 1759-1773, https://doi.org/10.5194/acp-17-1759-2017, 2017.

Berkemeier, T., Shiraiwa, M., Pöschl, U. and Koop, T.: Competition between water uptake and ice nucleation by glassy organic aerosol particles, Atmos. Chem. Phys., 14, 12513-12531, https://doi.org/10.5194/acp-14-12513-2014, 2014.

Bilde, M., Barsanti, K., Booth, M., Cappa, C. D., Donahue, N. M., Emanuelsson, E. U., McFiggans, G., Krieger, U. K., Marcolli, C., Topping, D., Ziemann, P., Barley, M., Clegg, S., Dennis-Smither, B., Hallquist, M., Hallquist, Å. M., Khlystov, A., Kulmala, M., Mogensen, D., Percival, C. J., Pope, F., Reid, J. P., Ribeiro da Silva, M. A. V., Rosenoern, T., Salo, K., Soonsin, V. P., Yli-Juuti, T., Prisle, N. L., Pagels, J., Rarey, J., Zardini, A. A. and Riipinen, I.: Saturation vapor pressures and transition enthalpies of low-volatility organic molecules of atmospheric relevance: from dicarboxylic acids to complex mixtures, Chem. Rev., 115, 4115-4156, https://doi.org/10.1021/cr5005502, 2015.

Bosse, D.: Diffusion, viscosity, and thermodynamics in liquid systems, Ph.D. thesis, https://kluedo.ub.uni-kl.de/frontdoor/deliver/index/docId/1691/file/PhD-Bosse-published.pdf, 2005.

Boyer, R. F.: Relationship of first-to second-order transition temperatures for crystalline high polymers, J. Appl. Phys., 25, 825-829, https://doi.org/10.1063/1.1721752, 1954.

Cao, W., Knudsen, K., Fredenslund, A. and Rasmussen, P.: Group-contribution viscosity predictions of liquid mixtures using UNIFAC-VLE parameters, Ind. Eng. Chem. Res., 32, 2088–2092, https://doi.org/10.1021/ie00021a034, 1993.

645 Capouet, M. and Müller, J.-F.: A group contribution method for estimating the vapour
646   pressures of α-pinene oxidation products, Atmos. Chem. Phys., 6, 1455-1467,
647   https://doi.org/10.5194/acp-6-1455-2006, 2006.

648 Cappa, C. D. and Jimenez, J. L.: Quantitative estimates of the volatility of ambient
649   organic aerosol, Atmos. Chem. Phys., 10, 5409-5424,
650   https://doi.org/10.5194/acp-10-5409-2010, 2010.

651 Carlton, A. G., de Gouw, J., Jimenez, J. L., Ambrose, J. L., Attwood, A. R., Brown, S.,
652   Baker, K. R., Brock, C., Cohen, R. C. and Edgerton, S.: Synthesis of the
653   southeast atmosphere studies: Investigating fundamental atmospheric chemistry
654   questions, Bull. Amer. Meteor. Soc., 99, 547-567,
655   https://doi.org/10.1175/BAMS-D-16-0048.1, 2018.

656 Cerully, K. M., Bougiatioti, A., Hite Jr, J. R., Guo, H., Xu, L., Ng, N. L., Weber, R. and
657   Nenes, A.: On the link between hygroscopicity, volatility, and oxidation state
658   of ambient and water-soluble aerosols in the southeastern United States, Atmos.
659   Chem. Phys., 15, 8679-8694, https://doi.org/10.5194/acp-15-8679-2015, 2015.

660 Champion, W. M., Rothfuss, N. E., Petters, M. D. and Grieshop, A. P.: Volatility and
661   viscosity are correlated in terpene secondary organic aerosol formed in a flow
662   reactor, Environ. Sci. Technol. Lett., 6, 513-519,
663   https://doi.org/10.1021/acs.estlett.9b00412, 2019.

664 Chenyakin, Y., Ullmann, D. A., Evoy, E., Renbaum-Wolff, L., Kamal, S. and Bertram,
665   A. K.: Diffusion coefficients of organic molecules in sucrose–water solutions
666   and comparison with Stokes–Einstein predictions, Atmos. Chem. Phys., 17,
667   2423-2435, https://doi.org/10.5194/acp-17-2423-2017, 2017.

668 Compernolle, S., Ceulemans, K. and Müller, J. F.: EVAPORATION: a new vapour
669   pressure estimation methodfor organic molecules including non-additivity and
670   intramolecular interactions, Atmos. Chem. Phys., 11, 9431-9450,
671   https://doi.org/10.5194/acp-11-9431-2011, 2011.

672 D'Ambro, E. L., Schobesberger, S., Gaston, C. J., Lopez-Hilfiker, F. D., Lee, B. H.,
673   Liu, J., Zelenyuk, A., Bell, D., Cappa, C. D., Helgestad, T., Li, Z., Guenther,
674   A., Wang, J., Wise, M., Caylor, R., Surratt, J. D., Riedel, T., Hyttinen, N., Salo,
675   V. T., Hasan, G., Kurtén, T., Shilling, J. E. and Thornton, J. A.: Chamber-based
676   insights into the factors controlling epoxydiol (IEPOX) secondary organic
677   aerosol (SOA) yield, composition, and volatility, Atmos. Chem. Phys., 19,
678   11253-11265, https://doi.org/10.5194/acp-19-11253-2019, 2019.

679 DeRieux, W.-S. W., Lakey, P. S. J., Chu, Y., Chan, C. K. K., Glicker, H., Smith, J. N.,
680   Zuend, A. and Shiraiwa, M.: Effects of phase state and phase separation on
681   dimethylamine uptake of ammonium sulfate and ammonium sulfate–sucrose
682   mixed particles, ACS Earth Space Chem., 3, 1268-1278,
683   https://doi.org/10.1021/acsearthspacechem.9b00142, 2019.

684 DeRieux, W. S. W., Li, Y., Lin, P., Laskin, J., Laskin, A., Bertram, A. K., Nizkorodov,
685   S. A. and Shiraiwa, M.: Predicting the glass transition temperature and viscosity

of secondary organic material using molecular composition, Atmos. Chem. Phys., 18, 6331-6351, https://doi.org/10.5194/acp-18-6331-2018, 2018.

Dette, H. P., Qi, M., Schröder, D. C., Godt, A. and Koop, T.: Glass-forming properties of 3-methylbutane-1,2,3-tricarboxylic acid and its mixtures with water and pinonic acid, J. Phys. Chem. A, 118, 7024-7033, https://doi.org/10.1021/jp505910w, 2014.

Dette, H. P. and Koop, T.: Glass formation processes in mixed inorganic/organic aerosol particles, J. Phys. Chem. A, 119, 4552-4561, https://doi.org/10.1021/jp5106967, 2015.

Ditto, J. C., Barnes, E. B., Khare, P., Takeuchi, M., Joo, T., Bui, A. A. T., Lee-Taylor, J., Eris, G., Chen, Y., Aumont, B., Jimenez, J. L., Ng, N. L., Griffin, R. J. and Gentner, D. R.: An omnipresent diversity and variability in the chemical composition of atmospheric functionalized organic aerosol, Commun. Chem., 1, https://doi.org/10.1038/s42004-018-0074-3, 2018.

Ditto, J. C., Joo, T., Khare, P., Sheu, R., Takeuchi, M., Chen, Y., Xu, W., Bui, A. A. T., Sun, Y., Ng, N. L. S. and Gentner, D. R.: Effects of molecular-level compositional variability in organic aerosol on phase state and thermodynamic mixing behavior, Environ. Sci. Technol., 53, 13009-13018, https://doi.org/10.1021/acs.est.9b02664, 2019.

Donahue, N., Robinson, A., Stanier, C. and Pandis, S.: Coupled partitioning, dilution, and chemical aging of semivolatile organics, Environ. Sci. Technol., 40, 2635-2643, https://doi.org/10.1021/es052297c, 2006.

Donahue, N., Epstein, S., Pandis, S. and Robinson, A.: A two-dimensional volatility basis set: 1. organic-aerosol mixing thermodynamics, Atmos. Chem. Phys., 11, 3303-3318, https://doi.org/10.5194/acp-11-3303-2011, 2011.

Evoy, E., Maclean, A. M., Rovelli, G., Li, Y., Tsimpidi, A. P., Karydis, V. A., Kamal, S., Lelieveld, J., Shiraiwa, M., Reid, J. P. and Bertram, A. K.: Predictions of diffusion rates of large organic molecules in secondary organic aerosols using the Stokes–Einstein and fractional Stokes–Einstein relations, Atmos. Chem. Phys., 19, 10073-10085, https://doi.org/10.5194/acp-19-10073-2019, 2019.

Faulhaber, A. E., Thomas, B. M., Jimenez, J. L., Jayne, J. T., Worsnop, D. R. and Ziemann, P. J.: Characterization of a thermodenuder-particle beam mass spectrometer system for the study of organic aerosol volatility and composition, Atmos. Meas. Tech., 2, 15-31, https://doi.org/10.5194/amt-2-15-2009, 2009.

Freedman, M. A.: Phase separation in organic aerosol, Chem. Soc. Rev., 46, 7694-7705, https://doi.org/10.1039/c6cs00783j, 2017.

Gervasi, N. R., Topping, D. O. and Zuend, A.: A predictive group-contribution model for the viscosity of aqueous organic aerosol, Atmos. Chem. Phys., 20, 2987-3008, https://doi.org/10.5194/acp-20-2987-2020, 2020.

Goldstein, A. H. and Galbally, I. E.: Known and unexplored organic constituents in the Earth's atmosphere, Environ. Sci. Technol., 41, 1514-1521, https://doi.org/10.1021/es072476p, 2007.

Gordon, M. and Taylor, J. S.: Ideal copolymers and the second-order transitions of synthetic rubbers. i. non-crystalline copolymers, J. Appl. Chem., 2, 493-500, https://doi.org/10.1002/jctb.5010020901, 1952.

Gorkowski, K., Preston, T. C. and Zuend, A.: RH-dependent organic aerosol thermodynamics via an efficient reduced-complexity model, Atmos. Chem. Phys., 19, 13383–13407, https://doi.org/10.5194/acp-2019-495, 2019a.

Gorkowski, K., Donahue, N. M., and Sullivan, R. C.: Aerosol optical tweezers constrain the morphology evolution of liquid-liquid phase-separated atmospheric particles, Chem, 6, 1-17, https://doi.org/10.1016/j.chempr.2019.1010.1018, 2019b.

Grayson, J. W., Zhang, Y., Mutzel, A., Renbaum-Wolff, L., Böge, O., Kamal, S., Herrmann, H., Martin, S. T. and Bertram, A. K.: Effect of varying experimental conditions on the viscosity of α-pinene derived secondary organic material, Atmos. Chem. Phys., 16, 6027-6040, https://doi.org/10.5194/acp-16-6027-2016, 2016.

Hallquist, M., Wenger, J., Baltensperger, U., Rudich, Y., Simpson, D., Claeys, M., Dommen, J., Donahue, N., George, C. and Goldstein, A.: The formation, properties and impact of secondary organic aerosol: current and emerging issues, Atmos. Chem. Phys., 9, 5155–5236, https://doi.org/10.5194/acp-9-5155-2009, 2009.

Hu, W. W., Campuzano-Jost, P., Palm, B. B., Day, D. A., Ortega, A. M., Hayes, P. L., Krechmer, J. E., Chen, Q., Kuwata, M., Liu, Y. J., de Sá, S. S., McKinney, K., Martin, S. T., Hu, M., Budisulistiorini, S. H., Riva, M., Surratt, J. D., St. Clair, J. M., Isaacman-Van Wertz, G., Yee, L. D., Goldstein, A. H., Carbone, S., Brito, J., Artaxo, P., de Gouw, J. A., Koss, A., Wisthaler, A., Mikoviny, T., Karl, T., Kaser, L., Jud, W., Hansel, A., Docherty, K. S., Alexander, M. L., Robinson, N. H., Coe, H., Allan, J. D., Canagaratna, M. R., Paulot, F. and Jimenez, J. L.: Characterization of a real-time tracer for isoprene epoxydiols-derived secondary organic aerosol (IEPOX-SOA) from aerosol mass spectrometer measurements, Atmos. Chem. Phys., 15, 11807-11833, https://doi.org/10.5194/acp-15-11807-2015, 2015.

Hu, W., Palm, B. B., Day, D. A., Campuzano-Jost, P., Krechmer, J. E., Peng, Z., de Sá, S. S., Martin, S. T., Alexander, M. L., Baumann, K., Hacker, L., Kiendler-Scharr, A., Koss, A. R., de Gouw, J. A., Goldstein, A. H., Seco, R., Sjostedt, S. J., Park, J. H., Guenther, A. B., Kim, S., Canonaco, F., Prévôt, A. S. H., Brune, W. H. and Jimenez, J. L.: Volatility and lifetime against OH heterogeneous reaction of ambient isoprene-epoxydiols-derived secondary organic aerosol (IEPOX-SOA), Atmos. Chem. Phys., 16, 11563-11580, https://doi.org/10.5194/acp-16-11563-2016, 2016.

Jain, S., Fischer, B. K. and Petrucci, A. G.: The Influence of absolute mass loading of secondary organic aerosols on their phase state, Atmosphere, 9, 131,

769   https://doi.org/10.3390/atmos9040131, https://doi.org/10.3390/atmos9040131,
770   2018.

771 Jimenez, J. L., Canagaratna, M. R., Donahue, N. M., Prevot, A. S. H., Zhang, Q., Kroll,
772   J. H., DeCarlo, P. F., Allan, J. D., Coe, H., Ng, N. L., Aiken, A. C., Docherty,
773   K. S., Ulbrich, I. M., Grieshop, A. P., Robinson, A. L., Duplissy, J., Smith, J.
774   D., Wilson, K. R., Lanz, V. A., Hueglin, C., Sun, Y. L., Tian, J., Laaksonen, A.,
775   Raatikainen, T., Rautiainen, J., Vaattovaara, P., Ehn, M., Kulmala, M.,
776   Tomlinson, J. M., Collins, D. R., Cubison, M. J., Dunlea, E. J., Huffman, J. A.,
777   Onasch, T. B., Alfarra, M. R., Williams, P. I., Bower, K., Kondo, Y., Schneider,
778   J., Drewnick, F., Borrmann, S., Weimer, S., Demerjian, K., Salcedo, D.,
779   Cottrell, L., Griffin, R., Takami, A., Miyoshi, T., Hatakeyama, S., Shimono, A.,
780   Sun, J. Y., Zhang, Y. M., Dzepina, K., Kimmel, J. R., Sueper, D., Jayne, J. T.,
781   Herndon, S. C., Trimborn, A. M., Williams, L. R., Wood, E. C., Middlebrook,
782   A. M., Kolb, C. E., Baltensperger, U. and Worsnop, D. R.: Evolution of organic
783   aerosols in the atmosphere, Science, 326, 1525-1529,
784   https://doi.org/10.1126/science.1180353, 2009.

785 Jöckel, P., Tost, H., Pozzer, A., Brühl, C., Buchholz, J., Ganzeveld, L., Hoor, P.,
786   Kerkweg, A., Lawrence, M., nbsp, G, Sander, R., Steil, B., Stiller, G., Tanarhte,
787   M., Taraborrelli, D., van Aardenne, J. and Lelieveld, J.: The atmospheric
788   chemistry general circulation model ECHAM5/MESSy1: consistent simulation
789   of ozone from the surface to the mesosphere, Atmos. Chem. Phys., 6, 5067-
790   5104, https://doi.org/10.5194/acp-6-5067-2006, 2006.

791 Kanakidou, M., Seinfeld, J., Pandis, S., Barnes, I., Dentener, F., Facchini, M.,
792   Dingenen, R. V., Ervens, B., Nenes, A. and Nielsen, C.: Organic aerosol and
793   global climate modelling: a review, Atmos. Chem. Phys., 5, 1053-1123,
794   https://doi.org/10.5194/acp-5-1053-2005, 2005.

795 Kauzmann, W.: The nature of the glassy state and the behavior of liquids at low
796   temperatures, Chem. Rev., 43, 219-256, https://doi.org/10.1021/cr60135a002,
797   1948.

798 Kidd, C., Perraud, V., Wingen, L. M. and Finlayson-Pitts, B. J.: Integrating phase and
799   composition of secondary organic aerosol from the ozonolysis of alpha-pinene,
800   Proc. Natl. Acad. Sci. U.S.A., 111, 7552-7557,
801   https://doi.org/10.1073/pnas.1322558111, 2014.

802 Knopf, D. A., Alpert, P. A. and Wang, B.: The role of organic aerosol in atmospheric
803   ice nucleation: a review, ACS Earth Space Chem., 2, 168-202,
804   https://doi.org/10.1021/acsearthspacechem.7b00120, 2018.

805 Kohl, I., Bachmann, L., Hallbrucker, A., Mayer, E. and Loerting, T.: Liquid-like
806   relaxation in hyperquenched water at $\leq$ 140 K, Phys. Chem. Chem. Phys., 7,
807   3210-3220, https://doi.org/10.1039/B507651J, 2005.

808 Koop, T., Bookhold, J., Shiraiwa, M. and Poschl, U.: Glass transition and phase state
809   of organic compounds: dependency on molecular properties and implications

810 for secondary organic aerosols in the atmosphere, Phys. Chem. Chem. Phys.,
811 13, 19238-19255, https://doi.org/10.1039/C1CP22617G, 2011.

812 Kostenidou, E., Karnezi, E., Hite Jr, J. R., Bougiatioti, A., Cerully, K., Xu, L., Ng, N.
813 L., Nenes, A. and Pandis, S. N.: Organic aerosol in the summertime southeastern
814 United States: components and their link to volatility distribution, oxidation
815 state and hygroscopicity, Atmos. Chem. Phys., 18, 5799-5819,
816 https://doi.org/10.5194/acp-18-5799-2018, 2018.

817 Krechmer, J. E., Day, D. A., Ziemann, P. J. and Jimenez, J. L.: Direct measurements of
818 gas/particle partitioning and mass accommodation coefficients in
819 environmental chambers, Environ. Sci. Technol., 51, 11867-11875,
820 https://doi.org/10.1021/acs.est.7b02144, 2017.

821 Krieger, U. K., Marcolli, C. and Reid, J. P.: Exploring the complexity of aerosol particle
822 properties and processes using single particle techniques, Chem. Soc. Rev., 41,
823 6631-6662, https://doi.org/10.1039/C2CS35082C, 2012.

824 Lambe, A. T., Onasch, T. B., Massoli, P., Croasdale, D. R., Wright, J. P., Ahern, A. T.,
825 Williams, L. R., Worsnop, D. R., Brune, W. H. and Davidovits, P.: Laboratory
826 studies of the chemical composition and cloud condensation nuclei (CCN)
827 activity of secondary organic aerosol (SOA) and oxidized primary organic
828 aerosol (OPOA), Atmos. Chem. Phys., 11, 8913-8928,
829 https://doi.org/10.5194/acp-11-8913-2011, 2011.

830 Lanz, V. A., Alfarra, M. R., Baltensperger, U., Buchmann, B., Hueglin, C. and Prévôt,
831 A. S. H.: Source apportionment of submicron organic aerosols at an urban site
832 by factor analytical modelling of aerosol mass spectra, Atmos. Chem. Phys., 7,
833 1503-1522, https://doi.org/10.5194/acp-7-1503-2007, 2007.

834 Lee, B.-H., Pierce, J. R., Engelhart, G. J. and Pandis, S. N.: Volatility of secondary
835 organic aerosol from the ozonolysis of monoterpenes, Atmos. Environ., 45,
836 2443-2452, https://doi.org/10.1016/j.atmosenv.2011.02.004, 2011.

837 Lessmeier, J., Dette, H. P., Godt, A. and Koop, T.: Physical state of 2-methylbutane-
838 1,2,3,4-tetraol in pure and internally mixed aerosols, Atmos. Chem. Phys., 18,
839 15841-15857, https://doi.org/10.5194/acp-18-15841-2018, 2018.

840 Li, Y., Pöschl, U. and Shiraiwa, M.: Molecular corridors and parameterizations of
841 volatility in the chemical evolution of organic aerosols, Atmos. Chem. Phys.,
842 16, 3327-3344, https://doi.org/10.5194/acp-16-3327-2016, 2016.

843 Li, Y. and Shiraiwa, M.: Timescales of secondary organic aerosols to reach equilibrium
844 at various temperatures and relative humidities, Atmos. Chem. Phys., 19, 5959-
845 5971, https://doi.org/10.5194/acp-19-5959-2019, 2019.

846 Lin, Y.-H., Zhang, Z., Docherty, K. S., Zhang, H., Budisulistiorini, S. H., Rubitschun,
847 C. L., Shaw, S. L., Knipping, E. M., Edgerton, E. S., Kleindienst, T. E., Gold,
848 A. and Surratt, J. D.: Isoprene epoxydiols as precursors to secondary organic
849 aerosol formation: acid-catalyzed reactive uptake studies with authentic
850 compounds, Environ. Sci. Technol., 46, 250-258,
851 https://doi.org/10.1021/es202554c, 2012.

852 Lin, Y.-H., Zhang, H., Pye, H. O. T., Zhang, Z., Marth, W. J., Park, S., Arashiro, M.,
853   Cui, T., Budisulistiorini, S. H., Sexton, K. G., Vizuete, W., Xie, Y., Luecken,
854   D. J., Piletic, I. R., Edney, E. O., Bartolotti, L. J., Gold, A. and Surratt, J. D.:
855   Epoxide as a precursor to secondary organic aerosol formation from isoprene
856   photooxidation in the presence of nitrogen oxides, Proc. Natl. Acad. Sci. U.S.A.,
857   110, 6718-6723, https://doi.org/10.1073/pnas.1221150110, 2013.

858 Liu, P., Li, Y. J., Wang, Y., Gilles, M. K., Zaveri, R. A., Bertram, A. K. and Martin, S.
859   T.: Lability of secondary organic particulate matter, Proc. Natl. Acad. Sci.
860   U.S.A., 113, 12643-12648, https://doi.org/10.1021/10.1021/acscentsci.
861   7b00452, 2016.

862 Liu, X., Day, D. A., Krechmer, J. E., Brown, W., Peng, Z., Ziemann, P. J. and Jimenez,
863   J. L.: Direct measurements of semi-volatile organic compound dynamics show
864   near-unity mass accommodation coefficients for diverse aerosols, Commun.
865   Chem., 2, https://doi.org/10.1038/s42004-019-0200-x, 2019.

866 Liu, Y., Wu, Z., Wang, Y., Xiao, Y., Gu, F., Zheng, J., Tan, T., Shang, D., Wu, Y.,
867   Zeng, L., Hu, M., Bateman, A. P. and Martin, S. T.: Submicrometer particles
868   are in the liquid state during heavy haze episodes in the urban atmosphere of
869   Beijing, China, Environ. Sci. Technol. Lett., 4, 427-432,
870   https://doi.org/10.1021/acs.estlett.7b00352, 2017.

871 Lopez-Hilfiker, F. D., Mohr, C., Ehn, M., Rubach, F., Kleist, E., Wildt, J., Mentel, T.
872   F., Lutz, A., Hallquist, M., Worsnop, D. and Thornton, J. A.: A novel method
873   for online analysis of gas and particle composition: description and evaluation
874   of a Filter Inlet for Gases and AEROsols (FIGAERO), Atmos. Meas. Tech., 7,
875   983-1001, https://doi.org/10.5194/amt-7-983-2014, 2014.

876 Lopez-Hilfiker, F. D., Mohr, C., D'Ambro, E. L., Lutz, A., Riedel, T. P., Gaston, C. J.,
877   Iyer, S., Zhang, Z., Gold, A., Surratt, J. D., Lee, B. H., Kurten, T., Hu, W. W.,
878   Jimenez, J., Hallquist, M. and Thornton, J. A.: Molecular composition and
879   volatility of organic aerosol in the southeastern U.S.: implications for IEPOX
880   derived SOA, Environ. Sci. Technol., 50, 2200-2209,
881   https://doi.org/10.1021/acs.est.5b04769, 2016.

882 Louvaris, E. E., Florou, K., Karnezi, E., Papanastasiou, D. K., Gkatzelis, G. I. and
883   Pandis, S. N.: Volatility of source apportioned wintertime organic aerosol in the
884   city of Athens, Atmos. Environ., 158, 138-147,
885   https://doi.org/10.1016/j.atmosenv.2017.03.042, 2017.

886 Loza, C. L., Coggon, M. M., Nguyen, T. B., Zuend, A., Flagan, R. C. and Seinfeld, J.
887   H.: On the mixing and evaporation of secondary organic aerosol components,
888   Environ. Sci. Technol., 47, 6173-6180, https://doi.org/ 10.1021/es400979k,
889   2013.

890 Marshall, F. H., Berkemeier, T., Shiraiwa, M., Nandy, L., Ohm, P. B., Dutcher, C. S.
891   and Reid, J. P.: Influence of particle viscosity on mass transfer and
892   heterogeneous ozonolysis kinetics in aqueous-sucrose-maleic acid aerosol,

Phys. Chem. Chem. Phys., 20, 15560-15573, https://doi.org/10.1039/c8cp01666f, 2018.

Mikhailov, E., Vlasenko, S., Martin, S. T., Koop, T. and Pöschl, U.: Amorphous and crystalline aerosol particles interacting with water vapor: conceptual framework and experimental evidence for restructuring, phase transitions and kinetic limitations, Atmos. Chem. Phys., 9, 9491-9522, https://doi.org/10.5194/acp-9-9491-2009, 2009.

Nizkorodov, S. A., Laskin, J. and Laskin, A.: Molecular chemistry of organic aerosols through the application of high resolution mass spectrometry, Phys. Chem. Chem. Phys., 13, 3612-3629, https://doi.org/10.1039/c0cp02032j, 2011.

O'Brien, R. E., Neu, A., Epstein, S. A., MacMillan, A. C., Wang, B., Kelly, S. T., Nizkorodov, S. A., Laskin, A., Moffet, R. C. and Gilles, M. K.: Physical properties of ambient and laboratory-generated secondary organic aerosol, Geophys. Res. Lett., 41, 4347-4353, https://doi.org/10.1002/2014GL060219, 2014.

O'Meara, S., Booth, A. M., Barley, M. H., Topping, D. and McFiggans, G.: An assessment of vapour pressure estimation methods, Phys.Chem.Chem.Phys., 16, 19453-19469, https://doi.org/10.1039/c4cp00857j, 2014.

Ortega, A. M., Hayes, P. L., Peng, Z., Palm, B. B., Hu, W., Day, D. A., Li, R., Cubison, M. J., Brune, W. H., Graus, M., Warneke, C., Gilman, J. B., Kuster, W. C., de Gouw, J., Gutiérrez-Montes, C. and Jimenez, J. L.: Real-time measurements of secondary organic aerosol formation and aging from ambient air in an oxidation flow reactor in the Los Angeles area, Atmos. Chem. Phys., 16, 7411-7433, 10.5194/acp-16-7411-2016, 2016.

Paciga, A., Karnezi, E., Kostenidou, E., Hildebrandt, L., Psichoudaki, M., Engelhart, G. J., Lee, B. H., Crippa, M., Prévôt, A. S. H., Baltensperger, U. and Pandis, S. N.: Volatility of organic aerosol and its components in the megacity of Paris, Atmos. Chem. Phys., 16, 2013-2023, https://doi.org/10.5194/acp-16-2013-2016, 2016.

Pajunoja, A., Hu, W., Leong, Y. J., Taylor, N. F., Miettinen, P., Palm, B. B., Mikkonen, S., Collins, D. R., Jimenez, J. L. and Virtanen, A.: Phase state of ambient aerosol linked with water uptake and chemical aging in the southeastern US, Atmos. Chem. Phys., 16, 11163-11176, https://doi.org/10.5194/acp-16-11163-2016, 2016.

Pajunoja, A., Malila, J., Hao, L., Joutsensaari, J., Lehtinen, K. E. and Virtanen, A.: Estimating the viscosity range of SOA particles based on their coalescence time, Aerosol Sci. Technol., 48, https://doi.org/10.1080/02786826.2013.870325, 2014.

Pankow, J. F.: An absorption model of gas-particle partitioning of organic-compounds in the atmosphere, Atmos. Environ., 28, 185-188, https://doi.org/10.1016/1352-2310(94)90093-0, 1994.

Pankow, J. F. and Asher, W. E.: SIMPOL.1: a simple group contribution method for predicting vapor pressures and enthalpies of vaporization of multifunctional organic compounds, Atmos. Chem. Phys., 8, 2773-2796, https://doi.org/10.5194/acp-8-2773-2008, 2008.

Perraud, V., Bruns, E. A., Ezell, M. J., Johnson, S. N., Yu, Y., Alexander, M. L., Zelenyuk, A., Imre, D., Chang, W. L., Dabdub, D., Pankow, J. F. and Finlayson-Pitts, B. J.: Nonequilibrium atmospheric secondary organic aerosol formation and growth, Proc. Natl. Acad. Sci. U.S.A., 109, 2836-2841, https://doi.org/10.1073/pnas.1119909109, 2012.

Petters, M. D. and Kreidenweis, S. M.: A single parameter representation of hygroscopic growth and cloud condensation nucleus activity, Atmos. Chem. Phys., 7, 1961-1971, https://doi.org/10.5194/acp-7-1961-2007, 2007.

Petters, S. S., Kreidenweis, S. M., Grieshop, A. P., Ziemann, P. J. and Petters, M. D.: Temperature- and humidity-dependent phase states of secondary organic aerosols, Geophys. Res. Lett., 46, https://doi.org/10.1029/2018GL080563, 2019.

Pöschl, U. and Shiraiwa, M.: Multiphase chemistry at the atmosphere-biosphere interface influencing climate and public health in the anthropocene, Chem. Rev., 115, 4440-4475, https://doi.org/10.1021/cr500487s, 2015.

Price, H. C., Mattsson, J. and Murray, B. J.: Sucrose diffusion in aqueous solution, Phys. Chem. Chem. Phys., 18, 19207-19216, https://doi.org/10.1039/c6cp03238a, 2016.

Pringle, K. J., Tost, H., Pozzer, A., Pöschl, U. and Lelieveld, J.: Global distribution of the effective aerosol hygroscopicity parameter for CCN activation, Atmos. Chem. Phys., 10, 5241-5255, https://doi.org/10.5194/acp-10-5241-2010, 2010.

Pye, H. O. T., Murphy, B. N., Xu, L., Ng, N. L., Carlton, A. G., Guo, H., Weber, R., Vasilakos, P., Appel, K. W., Budisulistiorini, S. H., Surratt, J. D., Nenes, A., Hu, W., Jimenez, J. L., Isaacman-VanWertz, G., Misztal, P. K. and Goldstein, A. H.: On the implications of aerosol liquid water and phase separation for organic aerosol mass, Atmos. Chem. Phys., 17, 343-369, https://doi.org/10.5194/acp-17-343-2017, 2017.

Reid, J. P., Bertram, A. K., Topping, D. O., Laskin, A., Martin, S. T., Petters, M. D., Pope, F. D. and Rovelli, G.: The viscosity of atmospherically relevant organic particles, Nat. Commun., 9, 956, https://doi.org/10.1038/s41467-018-03027-z, 2018.

Renbaum-Wolff, L., Grayson, J. W., Bateman, A. P., Kuwata, M., Sellier, M., Murray, B. J., Shilling, J. E., Martin, S. T. and Bertram, A. K.: Viscosity of α-pinene secondary organic material and implications for particle growth and reactivity, Proc. Natl. Acad. Sci. U.S.A., 110, 8014-8019, https://doi.org/10.1073/pnas.1219548110, 2013.

Riva, M., Chen, Y., Zhang, Y., Lei, Z., Olson, N. E., Boyer, H. C., Narayan, S., Yee, L. D., Green, H. S., Cui, T., Zhang, Z., Baumann, K., Fort, M., Edgerton, E.,

Budisulistiorini, S. H., Rose, C. A., Ribeiro, I. O., e Oliveira, R. L., dos Santos, E. O., Machado, C. M. D., Szopa, S., Zhao, Y., Alves, E. G., de Sá, S. S., Hu, W., Knipping, E. M., Shaw, S. L., Duvoisin Junior, S., de Souza, R. A. F., Palm, B. B., Jimenez, J.-L., Glasius, M., Goldstein, A. H., Pye, H. O. T., Gold, A., Turpin, B. J., Vizuete, W., Martin, S. T., Thornton, J. A., Dutcher, C. S., Ault, A. P. and Surratt, J. D.: Increasing isoprene epoxydiol-to-inorganic sulfate aerosol ratio results in extensive conversion of inorganic sulfate to organosulfur forms: implications for aerosol physicochemical properties, Environ. Sci. Technol., 53, 8682-8694, https://doi.org/10.1021/acs.est.9b01019, 2019.

Rothfuss, N. E. and Petters, M. D.: Influence of functional groups on the viscosity of organic aerosol, Environ. Sci. Technol., 51, 271-279, https://doi.org/10.1021/acs.est.6b04478, 2017.

Rovelli, G., Song, Y.-C., Maclean, A. M., Topping, D. O., Bertram, A. K. and Reid, J. P.: Comparison of approaches for measuring and predicting the viscosity of ternary component aerosol particles, Anal. Chem., 91, 5074-5082, https://doi.org/10.1021/acs.analchem.8b05353, 2019.

Saha, P. K., Khlystov, A., Yahya, K., Zhang, Y., Xu, L., Ng, N. L. and Grieshop, A. P.: Quantifying the volatility of organic aerosol in the southeastern US, Atmos. Chem. Phys., 17, 501-520, https://doi.org/10.5194/acp-17-501-2017, 2017.

Saha, P. K., Khlystov, A. and Grieshop, A. P.: Downwind evolution of the volatility and mixing state of near-road aerosols near a US interstate highway, Atmos. Chem. Phys., 18, 2139-2154, https://doi.org/10.5194/acp-18-2139-2018, 2018.

Saukko, E., Lambe, A. T., Massoli, P., Koop, T., Wright, J. P., Croasdale, D. R., Pedernera, D. A., Onasch, T. B., Laaksonen, A., Davidovits, P., Worsnop, D. R. and Virtanen, A.: Humidity-dependent phase state of SOA particles from biogenic and anthropogenic precursors, Atmos. Chem. Phys., 12, 7517-7529, https://doi.org/10.5194/acp-12-7517-2012, 2012.

Schmedding, R., Rasool, Q. Z., Zhang, Y., Pye, H. O. T., Zhang, H., Chen, Y., Surratt, J. D., Lee, B. H., Mohr, C., Lopez-Hilfiker, F. D., Thornton, J. A., Goldstein, A. H. and Vizuete, W.: Predicting secondary organic aerosol phase state and viscosity and its effect on multiphase chemistry in a regional scale air quality model, Atmos. Chem. Phys. Discuss., 2019, 1-59, https://doi.org/10.5194/acp-2019-900, 2019.

Schum, S. K., Zhang, B., Džepina, K., Fialho, P., Mazzoleni, C. and Mazzoleni, L. R.: Molecular and physical characteristics of aerosol at a remote free troposphere site: implications for atmospheric aging, Atmos. Chem. Phys., 18, 14017-14036, https://doi.org/10.5194/acp-18-14017-2018, 2018.

Seinfeld, J. H. and Pandis, S. N.: Atmospheric chemistry and physics - From air pollution to climate change, John Wiley & Sons, Inc., New York, 2006.

Shiraiwa, M., Ammann, M., Koop, T. and Poschl, U.: Gas uptake and chemical aging of semisolid organic aerosol particles, Proc. Natl. Acad. Sci. U.S.A., 108, 11003-11008, https://doi.org/10.1073/pnas.1103045108, 2011.

Shiraiwa, M. and Seinfeld, J. H.: Equilibration timescale of atmospheric secondary organic aerosol partitioning, Geophys. Res. Lett., 39, https://doi.org/10.1029/2012GL054008, 2012.

Shiraiwa, M., Zuend, A., Bertram, A. K. and Seinfeld, J. H.: Gas-particle partitioning of atmospheric aerosols: interplay of physical state, non-ideal mixing and morphology, Phys. Chem. Chem. Phys., 15, 11441-11453, https://doi.org/10.1039/C3CP51595H, 2013.

Shiraiwa, M., Berkemeier, T., Schilling-Fahnestock, K. A., Seinfeld, J. H. and Pöschl, U.: Molecular corridors and kinetic regimes in the multiphase chemical evolution of secondary organic aerosol, Atmos. Chem. Phys., 14, 8323-8341, https://doi.org/10.5194/acp-14-8323-2014, 2014.

Shiraiwa, M., Li, Y., Tsimpidi, A. P., Karydis, V. A., Berkemeier, T., Pandis, S. N., Lelieveld, J., Koop, T. and Pöschl, U.: Global distribution of particle phase state in atmospheric secondary organic aerosols, Nat. Commun., 8, 15002, https://doi.org/10.1038/ncomms15002, 2017.

Shrivastava, M., Cappa, C. D., Fan, J., Goldstein, A. H., Guenther, A. B., Jimenez, J. L., Kuang, C., Laskin, A., Martin, S. T., Ng, N. L., Petaja, T., Pierce, J. R., Rasch, P. J., Roldin, P., Seinfeld, J. H., Shilling, J., Smith, J. N., Thornton, J. A., Volkamer, R., Wang, J., Worsnop, D. R., Zaveri, R. A., Zelenyuk, A. and Zhang, Q.: Recent advances in understanding secondary organic aerosol: Implications for global climate forcing, Rev. Geophys., 55, 509-559, https://doi.org/10.1002/2016RG000540, 2017.

Slade, J. H., Ault, A. P., Bui, A. T., Ditto, J. C., Lei, Z., Bondy, A. L., Olson, N. E., Cook, R. D., Desrochers, S. J., Harvey, R. M., Erickson, M. H., Wallace, H. W., Alvarez, S. L., Flynn, J. H., Boor, B. E., Petrucci, G. A., Gentner, D. R., Griffin, R. J. and Shepson, P. B.: Bouncier particles at night: biogenic secondary organic aerosol chemistry and sulfate drive diel variations in the aerosol phase in a mixed forest, Environ. Sci. Technol., 53, 4977-4987, https://doi.org/10.1021/acs.est.8b07319, 2019.

Song, M., Liu, P. F., Hanna, S. J., Li, Y. J., Martin, S. T. and Bertram, A. K.: Relative humidity-dependent viscosities of isoprene-derived secondary organic material and atmospheric implications for isoprene-dominant forests, Atmos. Chem. Phys., 15, 5145-5159, https://doi.org/10.5194/acp-15-5145-2015, 2015.

Song, M., Liu, P. F., Hanna, S. J., Zaveri, R. A., Potter, K., You, Y., Martin, S. T. and Bertram, A. K.: Relative humidity-dependent viscosity of secondary organic material from toluene photo-oxidation and possible implications for organic particulate matter over megacities, Atmos. Chem. Phys., 16, 8817-8830, https://doi.org/10.5194/acp-16-8817-2016, 2016a.

Song, M., Maclean, A. M., Huang, Y., Smith, N. R., Blair, S. L., Laskin, J., Laskin, A., DeRieux, W. S. W., Li, Y., Shiraiwa, M., Nizkorodov, S. A. and Bertram, A. K.: Liquid-liquid phase separation and viscosity within secondary organic

aerosol generated from diesel fuel vapors, Atmos. Chem. Phys., 19, 12515–12529, https://doi.org/10.5194/acp-2019-367, 2019.

Song, Y. C., Haddrell, A. E., Bzdek, B. R., Reid, J. P., Bannan, T., Topping, D. O., Percival, C. and Cai, C.: Measurements and predictions of binary component aerosol particle viscosity, J. Phys. Chem. A, 120, 8123-8137, https://doi.org/10.1021/acs.jpca.6b07835, 2016b.

Stark, H., Yatavelli, R. L. N., Thompson, S. L., Kimmel, J. R., Cubison, M. J., Chhabra, P. S., Canagaratna, M. R., Jayne, J. T., Worsnop, D. R. and Jimenez, J. L.: Methods to extract molecular and bulk chemical information from series of complex mass spectra with limited mass resolution, Int. J. Mass Spectrom., 389, 26-38, https://doi.org/10.1016/j.ijms.2015.08.011, 2015.

Stark, H., Yatavelli, R. L., Thompson, S. L., Kang, H., Krechmer, J. E., Kimmel, J. R., Palm, B. B., Hu, W., Hayes, P. L. and Day, D. A.: Impact of thermal decomposition on thermal desorption instruments: advantage of thermogram analysis for quantifying volatility distributions of organic species, Environ. Sci. Technol., 51, 8491-8500, https://doi.org/10.1021/acs.est.7b00160, 2017.

Surratt, J. D., Chan, A. W. H., Eddingsaas, N. C., Chan, M., Loza, C. L., Kwan, A. J., Hersey, S. P., Flagan, R. C., Wennberg, P. O. and Seinfeld, J. H.: Reactive intermediates revealed in secondary organic aerosol formation from isoprene, Proc. Natl. Acad. Sci. U.S.A., 107, 6640-6645, https://doi.org/10.1073/pnas.0911114107, 2010.

Thomas, L. H., Meatyard, R., Smith, H. and Davies, G. H.: Viscosity behavior of associated liquids at lower temperatures and vapor pressures, J. Chem. Eng. Data, 24, 161-164, https://doi.org/10.1021/je60082a011, 1979.

Thompson, S. L., Yatavelli, R. L. N., Stark, H., Kimmel, J. R., Krechmer, J. E., Day, D. A., Hu, W., Isaacman-VanWertz, G., Yee, L., Goldstein, A. H., Khan, M. A. H., Holzinger, R., Kreisberg, N., Lopez-Hilfiker, F. D., Mohr, C., Thornton, J. A., Jayne, J. T., Canagaratna, M., Worsnop, D. R. and Jimenez, J. L.: Field intercomparison of the gas/particle partitioning of oxygenated organics during the Southern Oxidant and Aerosol Study (SOAS) in 2013, Aerosol Sci. Tech., 51, 30-56, https://doi.org/10.1080/02786826.2016.1254719, 2017.

Tsimpidi, A. P., Karydis, V. A., Pozzer, A., Pandis, S. N. and Lelieveld, J.: ORACLE (v1.0): module to simulate the organic aerosol composition and evolution in the atmosphere, Geosci. Model Dev., 7, 3153-3172, https://doi.org/10.5194/gmd-7-3153-2014, 2014.

US EPA: Estimation Programs Interface Suite^{TM} for Microsoft Windows v4.1, United States Environmental Protection Agency, Washington, DC, USA, 2015.

Vander Wall, A. C., Lakey, P. S. J., Rossich Molina, E., Perraud, V., Wingen, L. M., Xu, J., Soulsby, D., Gerber, R. B., Shiraiwa, M. and Finlayson-Pitts, B. J.: Understanding interactions of organic nitrates with the surface and bulk of organic films: implications for particle growth in the atmosphere, Environ. Sci.

Processes Impacts, 20, 1593-1610, https://doi.org/10.1039/C8EM00348C, 2018.

Virtanen, A., Joutsensaari, J., Koop, T., Kannosto, J., YliPirilä, P., Leskinen, J., Mäkelä, J. M., Holopainen, J. K., Pöschl, U., Kulmala, M., Worsnop, D. R. and Laaksonen, A.: An amorphous solid state of biogenic secondary organic aerosol particles, Nature, 467, 824-827, https://doi.org/10.1038/nature09455, 2010.

Xu, L., Suresh, S., Guo, H., Weber, R. J. and Ng, N. L.: Aerosol characterization over the southeastern United States using high-resolution aerosol mass spectrometry: spatial and seasonal variation of aerosol composition and sources with a focus on organic nitrates, Atmos. Chem. Phys., 15, 7307-7336, https://doi.org/10.5194/acp-15-7307-2015, 2015.

Xu, W., Xie, C., Karnezi, E., Zhang, Q., Wang, J., Pandis, S. N., Ge, X., Zhang, J., An, J., Wang, Q., Zhao, J., Du, W., Qiu, Y., Zhou, W., He, Y., Li, Y., Li, J., Fu, P., Wang, Z., Worsnop, D. R. and Sun, Y.: Summertime aerosol volatility measurements in Beijing, China, Atmos. Chem. Phys., 19, https://doi.org/10205-10216, 10.5194/acp-19-10205-2019, 2019.

Yatavelli, R. L. N., Mohr, C., Stark, H., Day, D. A., Thompson, S. L., Lopez-Hilfiker, F. D., Campuzano-Jost, P., Palm, B. B., Vogel, A. L., Hoffmann, T., Heikkinen, L., Äijälä, M., Ng, N. L., Kimmel, J. R., Canagaratna, M. R., Ehn, M., Junninen, H., Cubison, M. J., Petäjä, T., Kulmala, M., Jayne, J. T., Worsnop, D. R. and Jimenez, J. L.: Estimating the contribution of organic acids to northern hemispheric continental organic aerosol, Geophys. Res. Lett., 42, 6084-6090, https://doi.org/10.1002/2015gl064650, 2015.

Ye, Q., Robinson, E. S., Ding, X., Ye, P., Sullivan, R. C. and Donahue, N. M.: Mixing of secondary organic aerosols versus relative humidity, Proc. Natl. Acad. Sci. U.S.A., 113, 12649-12654, https://doi.org/10.1073/pnas.1604536113, 2016.

Ye, Q., Upshur, M. A., Robinson, E. S., Geiger, F. M., Sullivan, R. C., Thomson, R. J. and Donahue, N. M.: Following particle-particle mixing in atmospheric secondary organic aerosols by using isotopically labeled terpenes, Chem, 4, 318-333, https://doi.org/10.1016/j.chempr.2017.12.008, 2018.

Yli-Juuti, T., Pajunoja, A., Tikkanen, O.-P., Buchholz, A., Faiola, C., Väisänen, O., Hao, L., Kari, E., Peräkylä, O., Garmash, O., Shiraiwa, M., Ehn, M., Lehtinen, K. and Virtanen, A.: Factors controlling the evaporation of secondary organic aerosol from α-pinene ozonolysis, Geophys. Res. Lett., 44, 2562-2570, https://doi.org/10.1002/2016GL072364, 2017.

Zaveri, R. A., Shilling, J. E., Zelenyuk, A., Liu, J., Bell, D. M., D'Ambro, E. L., Gaston, C. J., Thornton, J. A., Laskin, A., Lin, P., Wilson, J., Easter, R. C., Wang, J., Bertram, A. K., Martin, S. T., Seinfeld, J. H. and Worsnop, D. R.: Growth kinetics and size distribution dynamics of viscous secondary organic aerosol, Environ. Sci. Technol., 52, 1191-1199, https://doi.org/10.1021/acs.est.7b04623, 2018.

1141 Zhang, Y., Sanchez, M. S., Douet, C., Wang, Y., Bateman, A. P., Gong, Z., Kuwata,
1142   M., Renbaum-Wolff, L., Sato, B. B., Liu, P. F., Bertram, A. K., Geiger, F. M.
1143   and Martin, S. T.: Changing shapes and implied viscosities of suspended
1144   submicron particles, Atmos. Chem. Phys., 15, 7819-7829,
1145   https://doi.org/10.5194/acp-15-7819-2015, 2015.
1146 Zhang, Y., Katira, S., Lee, A., Lambe, A. T., Onasch, T. B., Xu, W., Brooks, W. A.,
1147   Canagaratna, M. R., Freedman, A. and Jayne, J. T.: Kinetically controlled glass
1148   transition measurement of organic aerosol thin films using broadband dielectric
1149   spectroscopy, Atmos. Meas. Tech., 11, 3479–3490,
1150   https://doi.org/10.5194/amt-11-3479-2018, 2018.
1151 Zhang, Y., Nichman, L., Spencer, P., Jung, J. I., Lee, A., Heffernan, B. K., Gold, A.,
1152   Zhang, Z., Chen, Y., Canagaratna, M. R., Jayne, J. T., Worsnop, D. R., Onasch,
1153   T. B., Surratt, J. D., Chandler, D., Davidovits, P. and Kolb, C. E.: The cooling
1154   rate and volatility dependent glass forming properties of organic aerosols
1155   measured by Broadband Dielectric Spectroscopy, Environ. Sci. & Technol., 53,
1156   12366-12378, https://doi.org/10.1021/acs.est.9b03317, 2019.
1157 Zhou, S., Hwang, B. C. H., Lakey, P. S. J., Zuend, A., Abbatt, J. P. D. and Shiraiwa,
1158   M.: Multiphase reactivity of polycyclic aromatic hydrocarbons is driven by
1159   phase separation and diffusion limitations, Proc. Natl. Acad. Sci. U.S.A., 116,
1160   11658-11663, https://doi.org/10.1073/pnas.1902517116, 2019.
1161 Zobrist, B., Marcolli, C., Pedernera, D. and Koop, T.: Do atmospheric aerosols form
1162   glasses?, Atmos. Chem. Phys., 8, 5221-5244, https://doi.org/10.5194/acp-8-
1163   5221-2008, 2008.
1164 Zuend, A. and Seinfeld, J. H.: Modeling the gas-particle partitioning of secondary
1165   organic aerosol: the importance of liquid-liquid phase separation, Atmos. Chem.
1166   Phys., 12, 3857-3882, https://doi.org/10.5194/acp-12-3857-2012, 2012.
1167
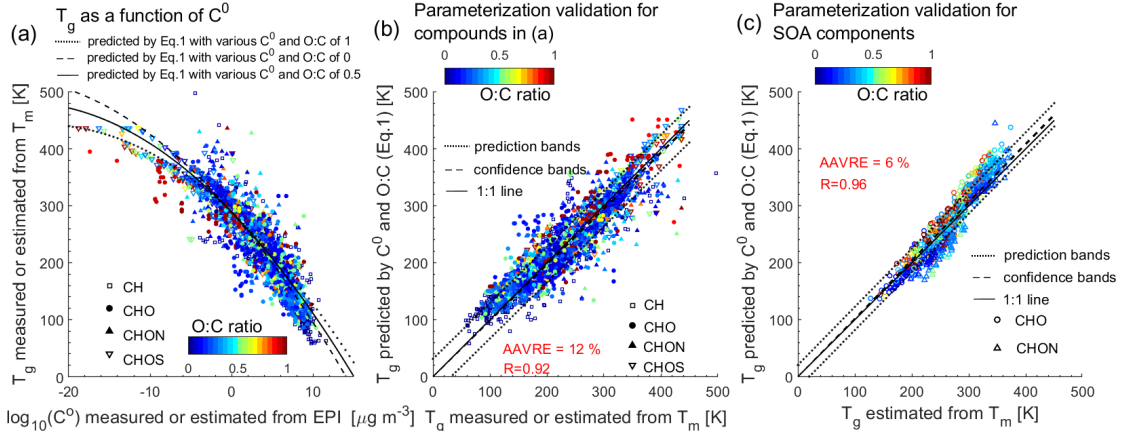
Figure 1. (a) T_g of organic compounds in the training dataset plotted against C^0. The lines show the predictions of T_g (Eq. 1) by C^0 and the O:C ratio of 0 (dashed), 0.5 (solid), and 1 (dotted). (b) Predicted T_g by C^0 and the O:C ratio (Eq. 1) for compounds shown in (a) compared to measured or otherwise estimated T_g from T_m. (c) Predicted T_g for SOA components (Shiraiwa et al., 2014) using Eq. (1) plotted against estimated T_g from T_m with the Boyer-Kauzmann rule. The correlation coefficient (R) and the average absolute value of the relative error (AAVRE) are shown. The dashed and dotted lines in (b) and (c) show 68% confidence and prediction bands, respectively.
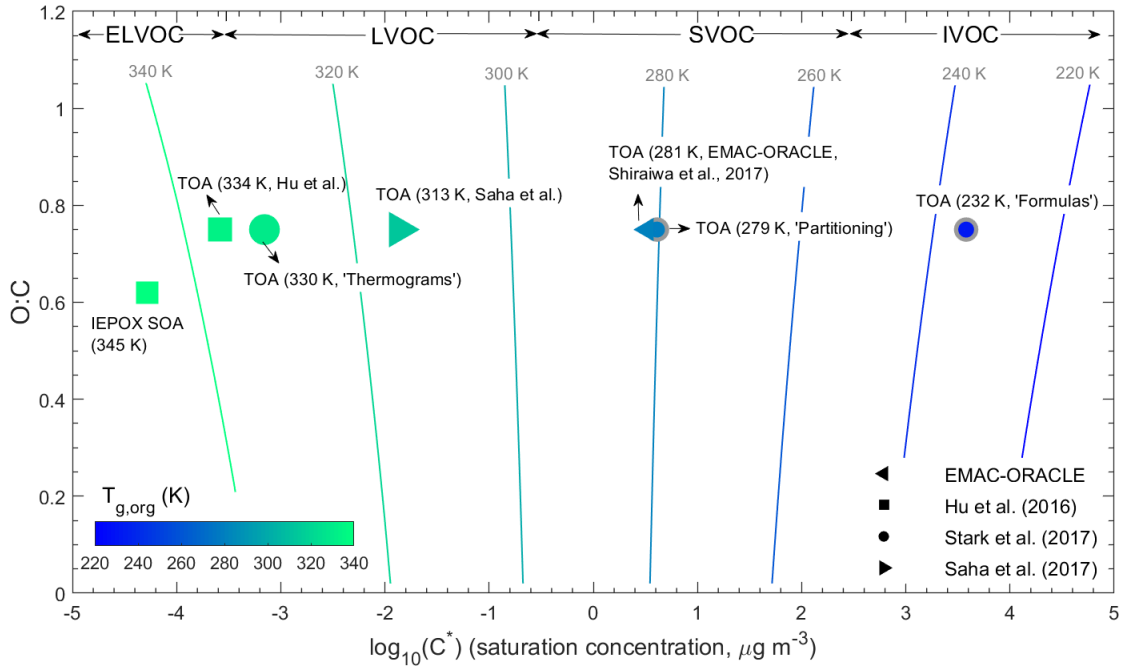
Figure 2. Predicted glass transition temperatures of organic aerosols under dry conditions ($T_{g,org}$) during the SOAS campaign placed into the 2-D VBS framework. The isopleths correspond to the T_g calculated using Eq. (1) with the effective saturation mass concentration (C^*) and the O:C ratio defined in the 2D-VBS. The markers represent the $T_{g,org}$ of total OA (TOA) and IEPOX SOA calculated from the volatility distributions simulated by a global chemical transport model EMAC-ORACLE (Shiraiwa et al., 2017) or measured during the SOAS campaign (Hu et al., 2016; Saha et al., 2017; Stark et al., 2017). Three methods ('Formulas', 'Partitioning', and 'Thermograms') are applied in Stark et al. (2017) to derive the C^* distributions, while the "Thermograms" method provides the most credible volatility distributions compared to 'Formulas' and 'Partitioning' (marker edge lines in gray).
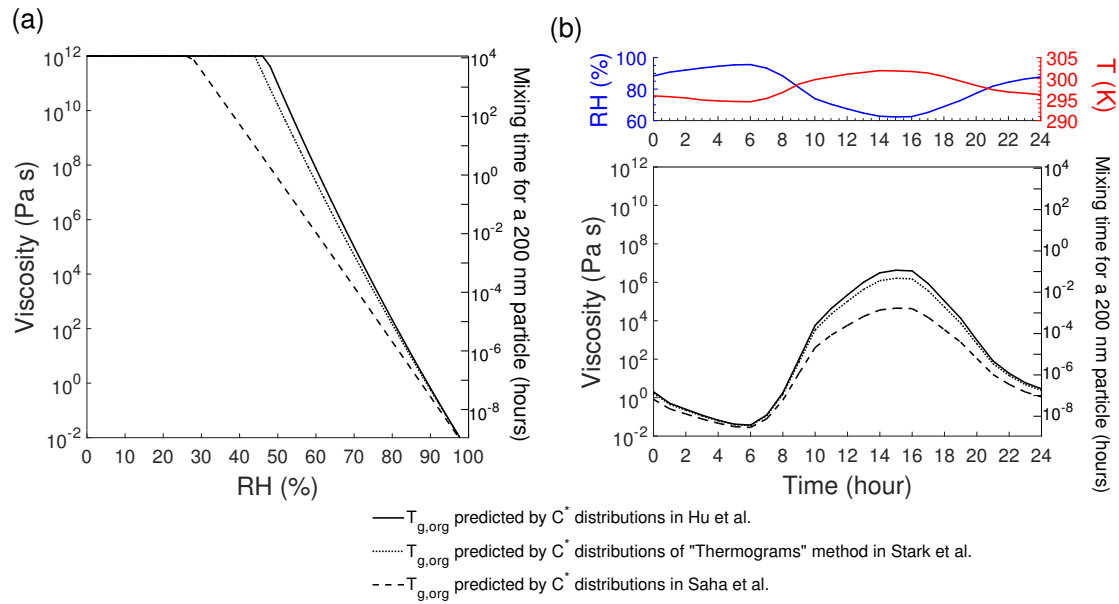
Figure 3. (a) Predicted viscosity of total OA measured during the SOAS campaign as a function of RH. (b) Diurnal variations of viscosity of total OA predicted employing the measured RH and T (Hu et al., 2016) during the SOAS campaign. $T_{g,org}$ are calculated using the volatility distributions measured in Hu et al., (2016), Saha et al. (2017), and the "Thermograms" method in Stark et al. (2017). Characteristic mixing timescales of organic molecules with the radius of 10^{-10} m within 200 nm particles are also shown in the right axis.

1199
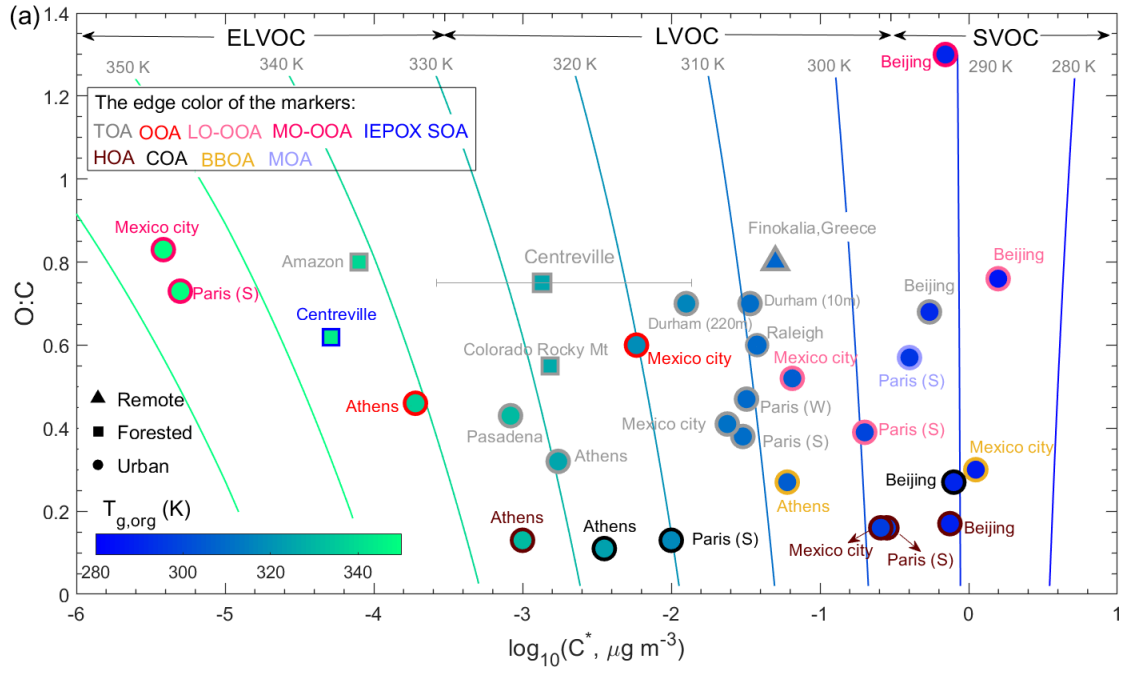
1200

Figure 4. Predicted glass transition temperatures of organic aerosols under dry conditions ($T_{g,org}$) at 11 sites. The fill color of the markers represents $T_{g,org}$ (a) or the O:C ratio (b). The marker edge color indicates the OA components identified via PMF of the AMS mass spectra. The isopleths in (a) correspond to T_g calculated using Eq. (1) with C^* and O:C defined in the 2D-VBS. The vertical error bars correspond to uncertainties in $T_{g,org}$ considering parameterization uncertainties and error propagation. The horizontal error bars for the Centreville site correspond to the upper and lower limits of the average $\log_{10}(C^*)$ calculated from different volatility distributions measured during the SOAS campaign (Hu et al., 2016; Saha et al., 2017; Stark et al., 2017).
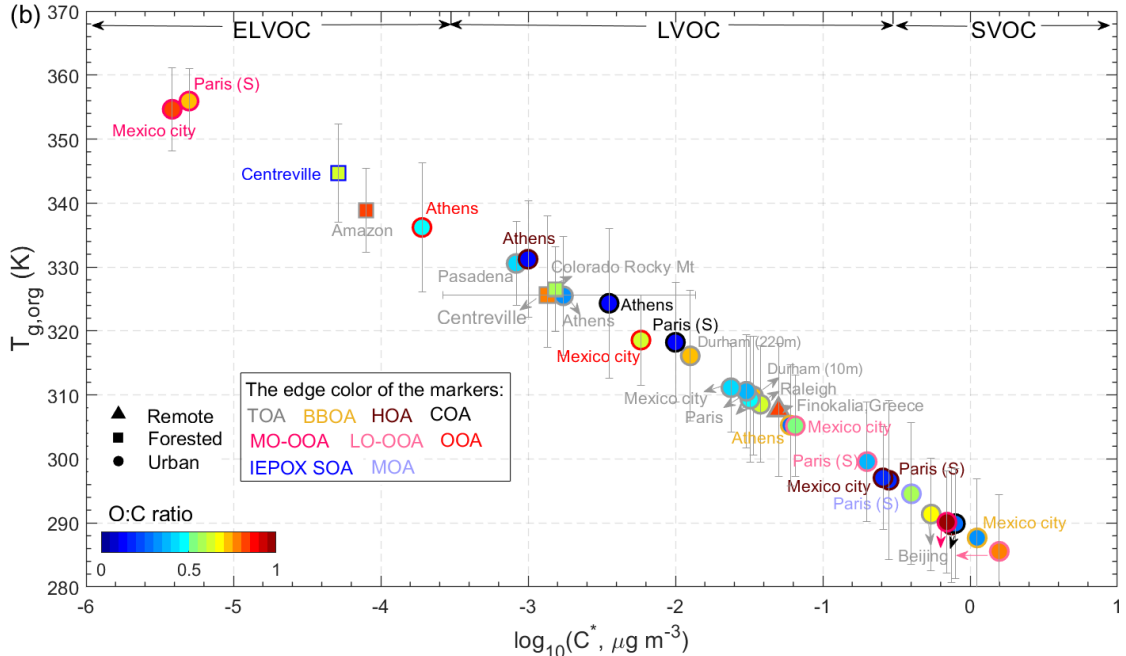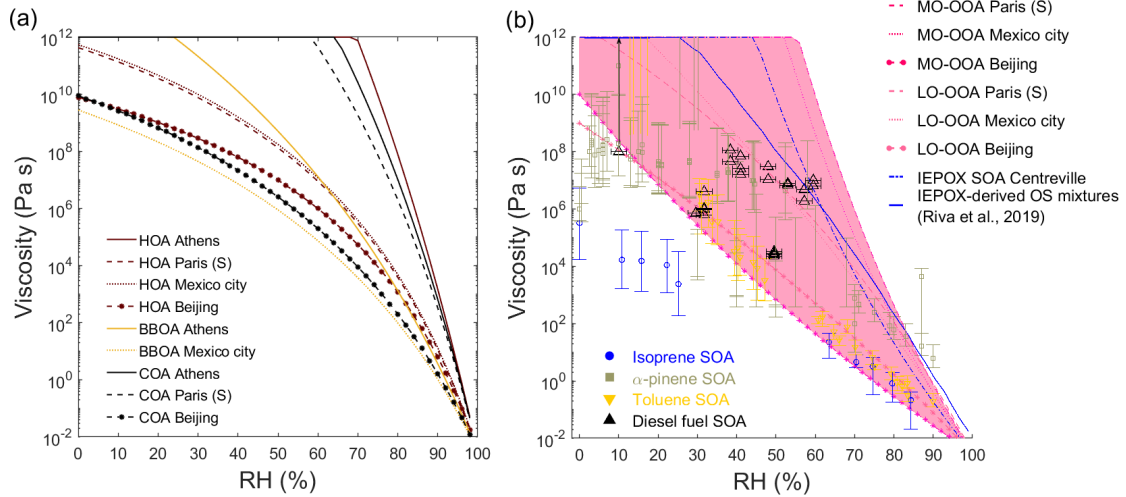
**Figure 5.** Predicted viscosity of (a) HOA, COA and BBOA and (b) LO-OOA, MO-OOA, and IEPOX SOA in different locations at 298 K as a function of RH. Experimentally measured viscosity of laboratory-generated SOA formed from isoprene (Song et al., 2015), α-pinene (Abramson et al., 2013; Renbaum-Wolff et al., 2013; Kidd et al., 2014; Pajunoja et al., 2014; Bateman et al., 2015; Zhang et al., 2015; Grayson et al., 2016; Petters et al., 2019), toluene (Song et al., 2016), and diesel fuel (Song et al., 2019) are also shown. Predicted viscosity of IEPOX-derived OS mixtures (solid blue line) is from Riva et al. (2019). Note that in case these OA factors are internally mixed with other components, the predicted viscosity would not represent real ambient complex organic mixtures.

**Figure 6.** (a) Global distributions of SOA annually averaged viscosity at the surface simulated by a global chemical transport model (Shiraiwa et al., 2017) with the viscosity predicted by measured volatility distributions at 11 global sites (triangle, square and circle represent remote, forested and urban sites, respectively, Table S3). The color code indicates viscosity in a log scale. (b) Predicted viscosity based on measured volatility distributions compared against the viscosity in global simulations. The error bars correspond to uncertainties in viscosities calculated from uncertainties in predicted $T_{g,org}$ shown in Fig. 4.
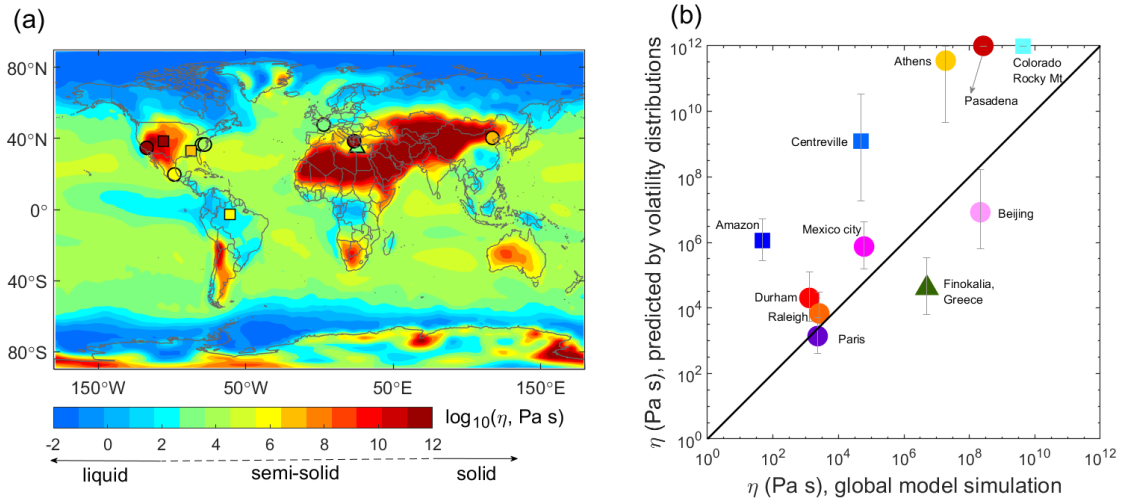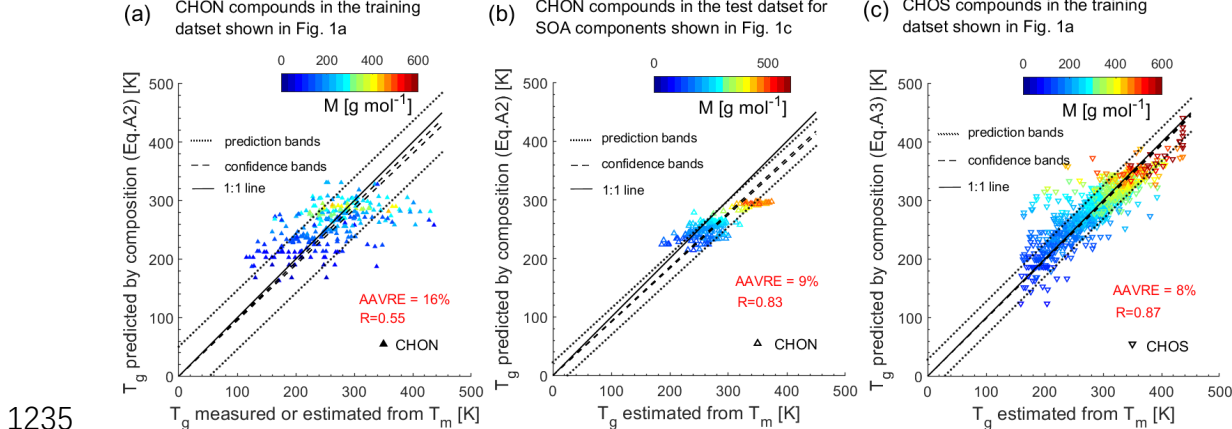
Figure A1. T_g predicted by elemental composition (Eq. A2) compared to (a) measured or otherwise estimated T_g by the Boyer-Kauzmann rule using measured T_m for CHON compounds in the training dataset and (b) estimated T_g by the Boyer-Kauzmann rule with T_m estimated by the EPI suite for CHON compounds in the test dataset for SOA components. (c) T_g predicted by elemental composition (Eq. A3) compared to estimated T_g by the Boyer-Kauzmann rule with T_m estimated by the EPI suite for CHOS compounds in the training dataset. The dashed and dotted lines show 68% confidence and prediction bands, respectively. The correlation coefficient (R) and the average absolute value of the relative error (AAVRE) are included in each figure legend.
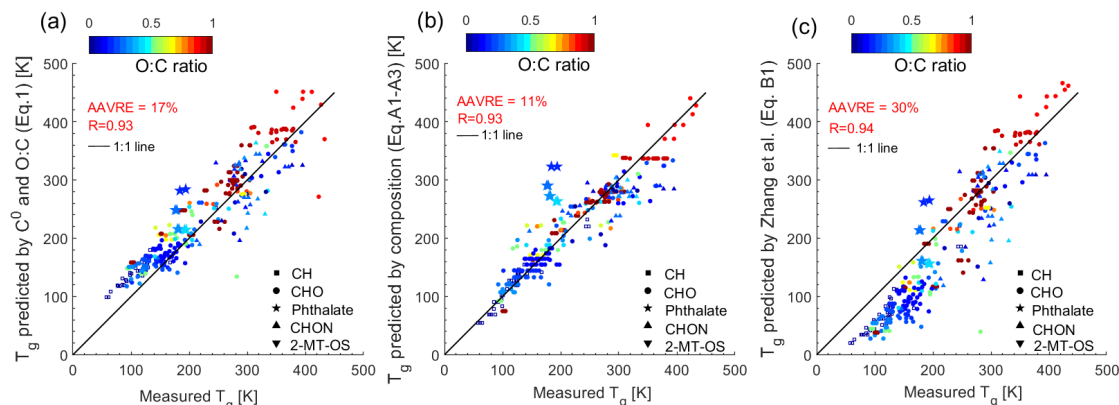
**Figure B1.** Comparison between measured T_g in the training dataset in Fig. 1a and T_g predicted by (a) C^0 and O:C (Eq. 1), (b) elemental composition (Eqs. A1-A3), and (c) the parameterization (Eq. B1) in Zhang et al. (2019). The solid line shows the 1:1 line. The correlation coefficient (R) and the average absolute value of the relative error (AAVRE) are included in each figure legend.

43
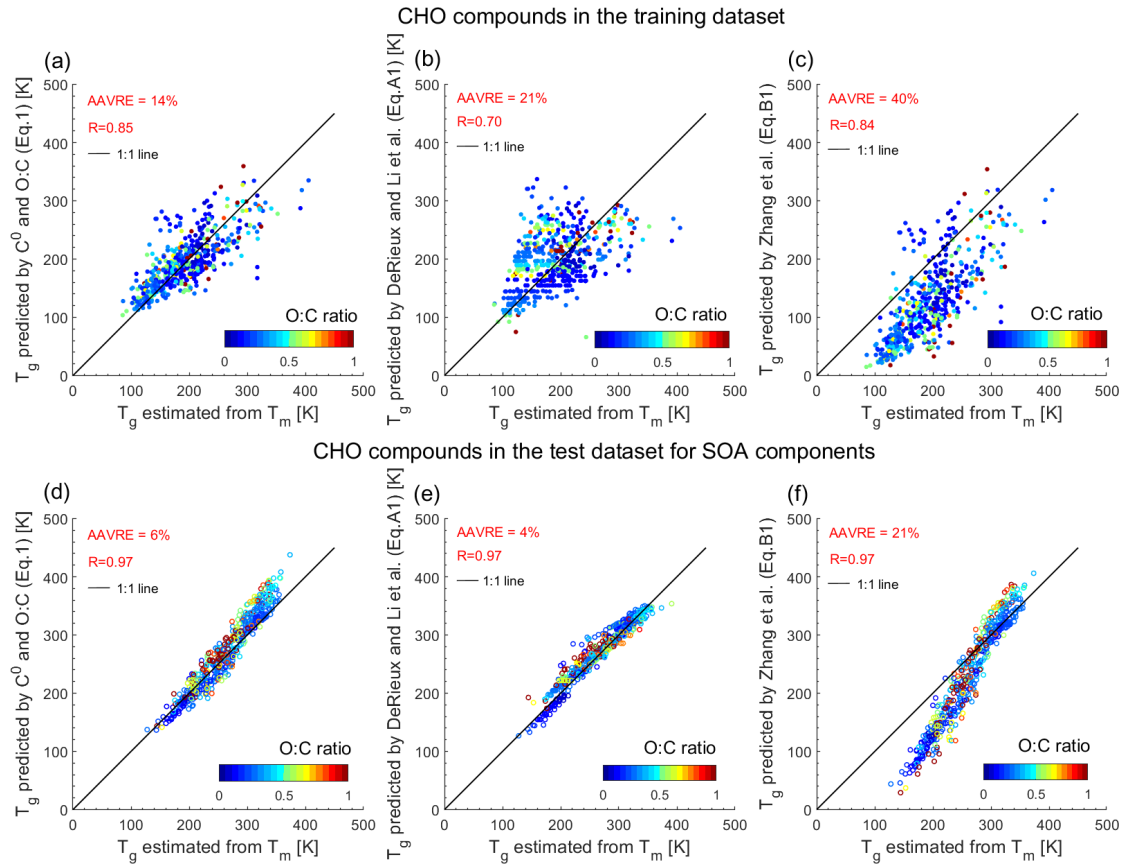
Figure B2. Predicted T_g by (a) C^0 and O:C (Eq. 1), (b) elemental composition (Eq. A1), and (c) the parameterization (Eq. B1) in Zhang et al. (2019) plotted against estimated T_g from T_m applying the Boyer-Kauzmann rule. CHO compounds in (a) – (c) included in the training dataset shown in Fig. 1a are with measured T_m and C^0 values; CHO compounds in (d) – (f) included in the test dataset for SOA components shown in Fig. 1c are with T_m and C^0 values estimated by the EPI Suite and the EVAPORATION model, respectively. The correlation coefficient (R) and the average absolute value of the relative error (AAVRE) are shown.